Reviews in Mineralogy & Geochemistry
Vol. 63, pp. 171-204, 2006

Time-resolved Neutron Diffraction Studies with Emphasis on Water Ices and Gas Hydrates

Werner F. Kuhs

Geowissenschaftliches Zentrum der Universität Göttingen
Abteilung Kristallographie
Goldschmidtstraße 1, 37077 Göttingen, Germany
e-mail: wf.kuhs@geo.uni-goettingen.de

Thomas C. Hansen

Institut Max von Laue-Paul Langevin, 6 rue Jules Horowitz, BP 156
38042 Grenoble Cedex 9, France
and
Geowissenschaftliches Zentrum der Universität Göttingen
Abteilung Kristallographie
Goldschmidtstraße 1, 37077 Göttingen, Germany
e-mail: hansen@ill.fr

INTRODUCTION

This chapter deals with applications of neutron diffraction to the understanding of transformation processes in geomaterials with a time-resolution from seconds to several days. The choice of neutrons rather than X-rays for such time-resolved studies is due to their specific advantages like e.g., the sensitivity to light elements, the detection of volume rather than surface phenomena or the low absorption in case of bulky sample environments. General features of diffractometers suitable for time-resolved studies are discussed and the high-flux diffractometer D20 at ILL is presented in some detail. Time-resolved processes usually are studied at non-ambient pressures and temperatures. The necessary sample environment needs to be provided and matched to the diffractometer set-up. Processes in water ices and gas hydrates are taken as examples and will be used to demonstrate the capabilities and limitations of the method.

Crystals are less static than what is usually suggested by immobile drawings of their atomic or molecular arrangements representing a time-space averaged picture of atomic positions as obtained from diffraction experiments. Rather, atoms or molecules exhibit thermal displacements and some even move inside the lattice as defects. These averaged displacements are described via atomic displacement parameters (e.g., Kuhs 2003) and are accessible also using diffraction techniques. Yet, there is even more movement in a crystal. Close to structural phase transitions the collective mobility of the constituents enables the formation of new structural arrangements to lower the free energy of the system (Redfern 2006, this volume). Such solid-solid transformations are not necessarily instantaneous, in particular when the new phase needs to be reconstructed by moving molecular and atomic constituents to a new position. Following such transitions is one of the main topics of this review.

Thermodiffractometry versus truly time-resolved studies

Phase transitions. If a material is capable of existing in more than one polymorphic form, the process of transformation from one polymorph to another is a phase transition (Redfern 2006, this volume). In the narrowest sense, these transitions are restricted to changes in structure only, in a wider one, the possibility of compositional changes is included. We shall

1529-6466/06/0063-0008$05.00 DOI: 10.2138/rmg.2006.63.8

call the latter a chemical reaction, to be distinguished from a purely structural, polymorphic transition. Time resolved work can be done in both cases and both cases are of interest here.

Thermodiffractometry. Sometimes, the formation of a new crystalline phase evolves in steps leading to short-lived intermediate phases, which may be accessed by diffractometry given that the data collection is sufficiently fast. A technique called thermodiffractometry (Pannetier 1985) gained popularity with the advent of one-dimensional position sensitive detectors, with which many powder diffraction patterns were taken while the samples were heated (or cooled) going through one or several phase transitions.

The term thermodiffractometry has been employed mainly for *in situ* diffraction studies on reversible phase transitions occurring with changing temperature. The temperature is continuously increased or decreased at a constant rate, and diffraction patterns are recorded during this temperature ramp at a constant pace. The dead time between two acquisitions has to be small, and the change of temperature during the acquisition of one pattern with sufficient counting statistics for later data treatment has to be sufficiently small.

In its narrowest sense, a thermodiffractometry experiment does not require a high time-resolution capacity, as the slope of the temperature ramp can be adapted to the necessary counting time. However, the term has been used as well, in a broader sense, for irreversible phase transitions or for experiments with a steep slope, not permitting to be in a thermodynamic but in a kinetic regime. One could, and sometimes has done, exploit the acquired data completely with respect to the kinetics of the phase transition.

Intermediate phases. In the frame of thermodiffractometry experiments in the latter sense, intermediate phases have unintentionally or purposely been observed (e.g., Kilcoyne and Manuel 2002) and studied, which have sometimes not been detected before (e.g., if the calorimetric fingerprint is not significant), and which may be only metastable and even not quenchable for *ex situ* studies. In this case the capability of doing time-resolved diffraction becomes important as the diffraction patterns must have sufficient counting rate for observation and acquisition of data sufficient for structural investigation in the short lapse of time the phase is present.

Truly time resolved studies

It is not the purpose to discuss thermodiffractometric experiments here, which have become a routine technique for exploring phase diagrams. We rather concentrate on truly time-resolved studies, in which a transformation process is followed at constant pressure and temperature to deduce kinetic information from diffraction data.

Studying the time dependency can be very instructive in giving quite detailed information on the mechanism of the transformation and delivering accurate reaction rate constants (see e.g., Levenspiel 1999). Time-resolved diffraction studies using powder samples give access to the relative amounts of the phases involved by a full pattern profile analysis (Knorr and Depmeier 2006, this volume). The formation of a new phase involves the formation of a critical nucleus and its subsequent growth. While the nucleus usually is so small that it yields only a very broad diffraction contribution, the growing crystallites produce increasingly sharp diffraction signals. The intensity of this evolving diffraction peak is proportional to the amount of new phase formed. A corresponding decrease of the Bragg peaks of the old phase should then be observed. The situation is more complicated in multiphase systems, in which constituents combine in heterogeneous chemical reactions to form new phases. Some of the constituents may be liquid or even gaseous. However, even in such cases the kinetics of the formation or decomposition of a crystalline phase may be followed by diffraction methods.

Meaningful information on the time-dependency of transformation processes in polycrystalline samples can only be obtained if the sample is sufficiently large to be representative. Transformations of different individual crystallites are not necessarily occurring

simultaneously. Therefore it is often necessary to investigate large samples to limit boundary effects and to observe averages of large ensembles. For highly absorbing materials neutrons give frequently a more representative picture of the bulk behavior of the material, while standard X-rays laboratory experiments are biased towards near-surface effects. Neutrons are generally better suited for such studies due to their lower absorption as compared to X-rays. Even when hard synchrotron X-rays could be used, the analyzed sample volume usually is limited to a few mm^3 and not necessarily representative for the whole sample.

Geomaterials are formed over a large range of time-scales. Some processes are fast and could be followed at relevant time-scales in neutron diffraction experiments. However, as the access to neutron facilities is limited, it is hardly possible to study processes on a timescale longer than a few days. Work at the home laboratory allows extending the time-scales but often gives less quantitative evidence for the ongoing changes when compared to neutron diffraction. Processes may take as long as thousands or millions of years. Obviously, such processes cannot be studied directly by any means. Fortunately, under certain assumptions, and given an appropriate model, neutron experiments at much shorter time-scales may be used to extrapolate to a different regime with slower rates, usually assuming an Arrhenius behavior of an underlying rate-determining activated process (Lasaga 1998). Reactions close to the melting or decomposition point of materials are usually fast due to the increased mobility of the constituents. For most minerals the corresponding high temperature conditions are difficult to reach, however. Undoubtedly, neutron diffraction has advantages here as it allows the use of bulky furnaces without much loss of data quality.

Other important geomaterials like ices and gas hydrates become mobile and reactive at much lower temperatures and can be studied fairly easily using neutrons. Neutrons of course provide relevant details concerning hydrogen positions and ordering, but also have advantages, in particular for gas hydrates, where elevated gas pressures are needed which can more easily be handled using neutron diffraction as compared to X-rays. The kinetics of ice transformation during structural phase transitions or the kinetics of gas hydrate formation and decomposition were not well known despite their importance in geology and planetology. Time-resolved neutron diffraction proved to be a major tool to change this situation.

In the following we will concentrate on time-resolved studies of ices and gas hydrates. We first describe specific issues of these systems concerning neutron diffraction. Then we proceed by providing details of the experimental set-ups and conclude by discussing several examples in some detail. We concentrate here on technical aspects as a detailed discussion of the scientific implications is beyond the scope of the chapter.

HYDROGENOUS SAMPLES

Hydrogen and X-ray diffraction

Hydrogen as the lightest element contributes much less to the scattered intensity from X-ray diffraction than all elements it is associated with. It is therefore difficult to localize in combination with heavier elements. Although this contrast problem is less dramatic in ice than in compounds with metals, we have to deal with roughly an order of magnitude less scattering intensity contributed from hydrogen compared to oxygen.

Additionally, for X-rays, scattering occurs with electrons, which are not well localized around the hydrogen atom's nucleus. The center of the electron distribution in ice shifts considerably towards the oxygen atom bound to hydrogen. Even if the data quality allows the determination of the center of the hydrogen electron density position, corrections are necessary to obtain the hydrogen core position. Such corrections require a good knowledge of the nature of the chemical bonding.

Hydrogen and neutron diffraction

Nuclear neutron scattering is not sensitive to the electron distribution but to the nature of the nuclei. The magnitude of the atomic form factor determining the contribution of an atom to the scattered intensity is not a simple function of the number of protons and neutrons of a particular scattering nucleus. Apart from some exceptions, these form factors are in the same order of magnitude for all isotopes, therefore we do not have to struggle with the inherent imbalance problem of X-ray diffraction.

Incoherent scattering. In many cases we have to deal with incoherent scattering that does not carry positional information in contrast to coherent scattering. For structural diffraction work, we must consider incoherent scattering as an unwanted background contribution. Reasons for a high incoherent scattering cross section are mixtures of isotopes with strongly different scattering lengths b or, more likely, isotopes with strongly different scattering lengths b_- and b_+ for both possible spin orientations (Parise 2006a, this volume).

The dominant naturally occurring isotope of hydrogen is ^{1}H (99.985%), which has an incoherent scattering length of b_{inc} = 25.274 fm (Sears 1992). Consequently, hydrogen has an incoherent cross section of σ_{inc} = 80.27 barns (1 barn = 10^{-28} m), which is the highest one of all stable elements and isotopes, apart from three heavily absorbing samarium and gadolinium isotopes and the element gadolinium itself. The coherent scattering length of the element is b_{coh} = −3.739 fm and the cross section σ_{coh} = 1.7568 barns, which is rather low (similar to a weak scatterer like titanium, oxygen has a four times higher cross section, iron and nickel have a more than ten times higher one).

In addition to the extremely unfavorable signal to background ratio, the incoherent scattering contributes to an efficient absorption although the cross section for true absorption of hydrogen is relatively small. Any neutron scattered incoherently and afterwards scattered coherently will no longer be detected correctly in a diffraction experiment. On the other hand, coherently scattered neutrons are likely to experience incoherent scattering before leaving the sample causing deflections from the ideal direction from the point of view of a diffraction experiment. This efficient absorption depends on the wavelength λ and even on the chemical environment of the hydrogen atoms. Howard et al. (1987) measured the efficient absorption cross section, using a single crystal of a particular compound, to be $\sigma_H(\lambda)$/barns = 19.2(5)λ/Å + 20.6(9).

As a further drawback, especially in constant wavelength neutron powder diffraction experiments on larger samples, multiple scattering may become important which will derive the coherently diffracted neutron's path from the ideal one. This leads to a considerable broadening of all diffraction peaks in the powder diffraction pattern and thus lowers the angular resolution. Thus the determination of peak intensities becomes less precise.

Deuteration. One way to avoid this difficulty is the replacement of natural hydrogen with its isotope deuterium (^{2}H or D), called deuteration. Full deuteration is usually the best choice but cannot always be achieved due to experimental and/or financial reasons. If it is only for background and absorption reduction the replacement of a maximum of hydrogen against deuterium is aimed at. If detailed structural information on a hydrogen position is needed, one must aim for complete deuteration. In the case of partial deuteration, the exchange ratio should be known from the synthesis procedure or be determined by some means. This can be achieved e.g., by spectroscopy, by accurate density measurements of the constituents or by a crystallographic refinement of positional occupancies (see e.g., Chazallon and Kuhs 2002). Deuterium has a coherent scattering length of 6.671 fm, a coherent cross section of 5.592 barns. The different sign of the coherent scattering length means, that the corresponding scattering contributions of ^{1}H and ^{2}H will partly or fully annihilate when placed statistically on one crystallographic position. An occupation of such a site at a ratio of ^{2}H to ^{1}H of 3.739/6.671 will make it invisible to diffraction (35.9% ^{2}H and 64.1% ^{1}H).

A major drawback of deuteration, beside problems of feasibility, is the physico-chemical isotopic difference of hydrogen and deuterium. Normally, different isotopes of the same element behave chemically identically; there are only tiny mass-related differences in the thermodynamic and kinetic behavior of isotopic compounds. However, in the case of hydrogen, this mass difference is important, deuterium is a factor of about two heavier. Moreover, quantum effects lead to a better localization of the deuteron with a resulting slightly weaker H-bond for the deuterated compound translating into larger lattice constants (Röttger et al 1994). The molecular translational und librational motion is considerably reduced in the deuterated compound (corresponding to the relevant reduced masses) which in turn affects the localized and collective motions of water molecules. This is expressed, for example in the melting point of water ice, which is, slightly varying with pressure, several degrees higher for D_2O than for H_2O. Further to these thermodynamic effects, the kinetic constants differ considerably for natural and deuterated samples. The water molecule's local mobility in hydrogenated and deuterated ices Ih differs as evidenced in dielectric relaxation, the deuterated compound having a longer relaxation time (Johari 1976; Johari and Jones 1976, 1978). Although the role of water mobility in the clathration reaction or in the accompanying gas- and water- mass transport is not clear, the established differences suggest that the hydrate formation kinetics in the H_2O- and D_2O-systems could be different. This difference has been investigated by Staykova et al. (2003) and found to be rather small. Dramatic differences in the transition behavior between hydrogenated and deuterated systems could be expected when proton tunneling is involved (e.g., Matsuo 2003). Such a transition is likely to take place e.g., when approaching high pressure ice X (e.g., Pruzan et al. 2003), presently outside reach for neutrons due to the very high pressures needed. At more moderate pressures proton tunneling may also occur in other ices when ionic defects are present (Petrenko and Whitworth 1999), however the role of proton tunneling for kinetic phenomena remains largely unexplored.

Annular sample containers. In order to study the thermodynamics and the kinetics of natural samples directly without extrapolating data from deuterated samples, one has to take measures to reduce absorption and multiple scattering. In neutron powder diffraction experiments conducted in Debye-Scherrer geometry with a normally cylindrical sample in transmission, this can be achieved by using a double-walled sample can instead of a simple cylinder. The absorbing sample then has not a solid radius of, e.g., 2 to 10 mm, but is distributed cylindrically around an inner, hollow cylinder of a radius between, e.g., 2 and 5 mm with a thickness of 0.5 to 2 mm. With such a geometry, the incident and diffracted beam have roughly the same path length for all diffraction angles.

In the case of a solid cylinder, the path length is in the order of the sample diameter for low diffraction angles and distributed from close to zero to up to about twice the diameter for high diffraction angles. For strongly absorbing samples this means an increase of diffracted intensity from low to high angles, which can be—in principle—corrected for. However, this correction presents some major difficulties, especially when the efficient absorption coefficient cannot be calculated at high precision (which is the case for hydrogen as shown by Howard et al. 1987): There is an enormous correlation between the refinable absorption correction coefficients with structural parameters such as atomic displacement parameters, both, modulating the diffraction intensity from low to high angles. Even if the absorption correction is successful, the loss of information at low angles remains an insurmountable handicap for structural work.

The use of annular sample containers provides a more equal intensity distribution over the whole angular range with less need for absorption correction and a corresponding reduction of parameter correlations. Schmitt and Ouladdiaf (1998) provide an algorithm and a computer program for performing this correction.

The outer radius R and the ratio between the inner and the outer radius, ρ, need careful optimization, as a maximum radius cannot be exceeded for instrumental reasons (i.e., decrease

of angular resolution) and as a minimum distance between the inner and the outer wall of the sample needs to be respected for reasons of mechanical feasibility. The equivalent radius R_{eq} of a full cylindrical sample with the same volume is given by $R_{eq}=R\cdot(1-\rho^2)^{1/2}$. The diffraction intensity gain at low diffraction angles can be very high (e.g., 15 for $\theta \approx 0°$ and $\mu R \approx 18$ with the linear absorption coefficient μ). For a full cylindrical sample, the optimized radius R_{opt} is given by $\mu R_{opt} \approx 1.5$ for $\theta \approx 0°$.

Finally, one should not forget that relatively long counting times or high incident neutron fluxes are necessary when working with non-deuterated hydrogenous samples: Even if one masters the problem of efficient absorption (and together with it the peak broadening due to multiple scattering), the problem of an extremely unfavorable low signal to background ratio remains. Only with deuteration incoherent scattering can be completely avoided, but the use of a high intensity diffractometer may produce useful data even under such unfavorable conditions in a reasonable measuring time. In the case of clathrate hydrate formation discussed below we found a decrease of precision of the refined phase fraction by roughly a factor of 40 when going from a partly deuterated CH_4-D_2O system to a fully hydrogenated CH_4-H_2O system, still far sufficient to refine meaningful phase fractions (Staykova et al. 2003).

INSTRUMENTS

Instrumentation at ILL

The ILL high flux reactor provides the world's highest thermal neutron flux as required for time-resolved experiments, particularly on hydrogen compounds. Two high-intensity powder diffractometers are of main interest D1B and D20 and were used in many of the experiments described below. They will be discussed in some detail.

The D1B powder diffractometer with a multi-wire gas chamber detector was used in the 1970's for the first truly time-resolved neutron diffraction experiments (Riekel and Schöllhorn 1976). The one-dimensional, curved position sensitive detector (PSD) covers a $\Delta 2\theta = 80°$ range of diffraction with a detector resolution of 0.1°.

The successor of D1B (Convert et al. 1998, 2000; Hansen 2004) is the instrument D20 that provides a much higher flux at the sample position. To achieve a high, detected intensity, a stationary, curved linear PSD covers the whole 2θ range (Convert et al. 1997). The high detection stability of the micro-strip gas chamber detector enables D20 also to accomplish high precision in intensity measurement. Several monochromators are available.

A vertically focusing graphite monochromator provides $\lambda \approx 2.41$ Å at a take-off angle of 42° and is equipped with graphite filters to suppress harmonics. Alternatively a vertically and horizontally focusing copper monochromator Cu (200) in transmission geometry provides a monochromatic neutron beam with wavelengths of $\lambda \approx 0.82, 0.88, 0.94$ Å at take-off angles of 26°, 28° or 30°. A second copper focusing monochromator Cu (200) in transmission provides $\lambda \approx 1.3$ Å at a take-off angle of 42°; this configuration is shown in Figure 1. At $\lambda = 1.3$ Å the monochromatic beam has its highest flux of about 10^8 n·cm^{-2}·s^{-1}. Soller collimators allow to reduce the divergence of the incident polychromatic beam (27′) to $\alpha_1 = 10'$ or 20′. A germanium monochromator with variable vertical focusing allows obtaining higher resolution at higher take-off angles (65±2°, 90±2°, 118° and 120°, shown in Fig. 2).

The PSD of aluminum has a useful angular aperture of 153.6° (2θ). The detection zone is about 4 m long and 15 cm high. The gas filling of 3 bars ^{3}He and 1 bar CF_4 and the detection gap of 5 cm result in a neutron detection efficiency from 60% ($\lambda = 0.8$ Å) to 90% (2.4 Å). Each detector plate of electronically conducting glass (Oed 1988) carries 32 cells, 2.568 mm in size (0.1°), and composed of two basic chromium micro-strips (anodes and cathodes). To cover continuously 153.6°, the PSD is composed of 48 juxtaposed, precisely cut plates in a polygonal

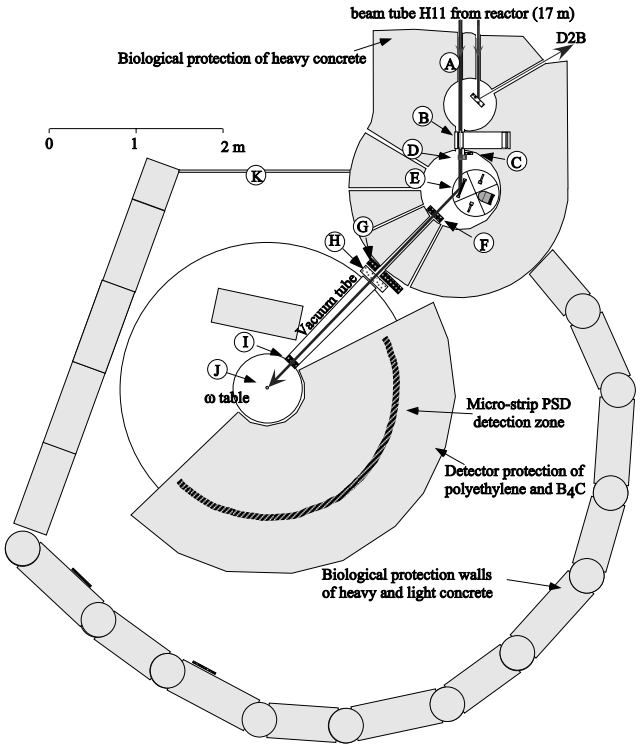

Figure 1. Schema of D20 in "high flux" configuration (take-off angle 42°). A: incident thermal neutron beam, B: optional 10' Soller collimator, C: primary fast thermal neutron beam shutter, D: highly oriented pyrolytic graphite (HOPG) filter, E: monochromator changer with HOPG (002) monochromator in beam, F: slits, G: secondary beam shutter, H: neutron beam monitor, I: slits, J: sample position, K: access gate.

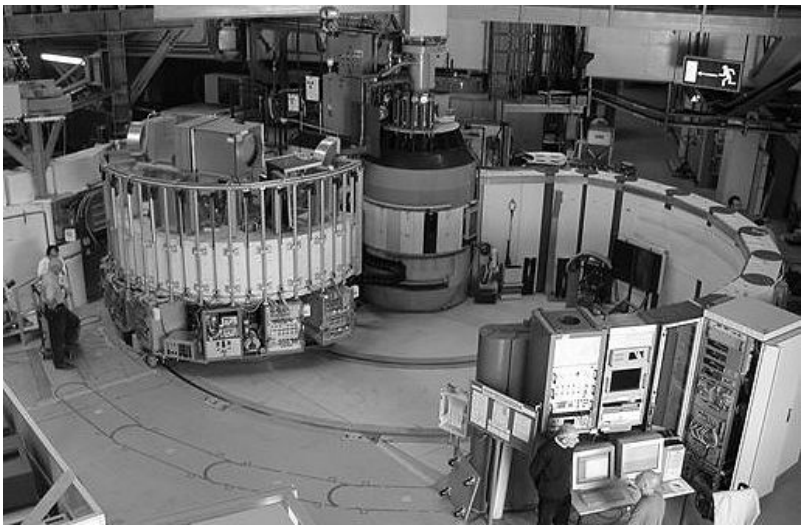

Figure 2. D20 at 120° take-off angle (high resolution configuration). A part of the biological concrete protection wall is not in place. In the front the instrument control electronics. The detector is seen from behind, its counting chain being hidden behind mountable, neutron-shielding doors of polyethylene and boron carbide. Below the detector, on the movable platform, the data acquisition system is visible.

arrangement with a radius of 1471 mm, each plate covering 3.2°. The 1536 cells are connected to amplifiers and discriminators and anti-coincidence circuits (CLET). A cell, whose amplifier signal passed first the discriminator threshold, inhibits its neighbors for 1.5 μs, avoiding double detection.

This makes D20 an ideal tool for *in situ* diffraction studies with time constants even below a second. Its high intensity enables the use of complex sample environments, as the high count-rate may level out low signal-to-noise ratios. D20's high precision in intensity measurement is needed for differential measurements and studies on liquid and amorphous systems. The different options described above provide a large choice in Q-space, resolution, wavelength (0.8 to 2.4 Å), and flux. The continuous and simultaneous detection of series of complete diffraction patterns is necessary for systematic investigations of phase transitions during variation of a parameter such as pressure or temperature. The structural evolution of solids during a chemical reaction can be studied *in situ* with single diffraction patterns of down to 400 ms in highest intensity configuration, allowing quantifying short-living intermediate phases and elucidate subtle structural changes. High-resolution powder diffraction patterns can be obtained in a few minutes when the highest take-off angle is used.

Faster, but cyclic phenomena are observable in a stroboscopic data acquisition mode (Convert et al. 1990). A reversible process, which is reproducible in a cyclic, repeated way, can be observed using *stroboscopy*, allowing for a much better time-resolution, i.e., the shortest possible time slice of the phenomenon to be observed. This is possible by synchronizing a series of sequential acquisitions (*slices*) with the cycling of the observed process. The results of these acquisitions from corresponding slices in different cycles cumulate electronically in a register. The final data set corresponds then to one cycle of the process, but the counting rate for each data acquisition slice is as many times higher than there were cycles measured. One obtains sufficient counting statistics for a series of slices after each synchronization-cycle by repeating a sufficient number of individual cycles and accumulating the counting rates of corresponding slices. Unfortunately, for various reasons one cannot go for shorter and shorter slices and correspondingly higher cycling frequencies. There are electronic limitations to provide a good synchronization over a large number of cycles without any deviation, e.g., due to fatigue phenomena. The principal limitation, however, is due to the finite velocity of neutrons, resulting in uncertainty about the time of the scattering event in the sample of some dimension, and of the detection event in the commonly used gas chamber detectors. Compared to this effect, the $\Delta\lambda/\lambda$ distribution to the time-resolution is negligible. Time resolution is thus limited by the travel time of neutrons through sample and detection gap, at D20 about 10 μs. Brown et al. (1998, 2000) have used stroboscopic acquisitions for rheologic investigations of orientation changes of flat or rod like particles, suspended in water, during laminar flow.

A radial oscillating collimator with a focus aperture of 22 mm and an angular coverage of 156° in 2θ permits the use of most types of sample environment without any background contributions from, e.g., aluminum cryostat-calorimeters or niobium heating elements. D20 has dedicated sample environment devices like an electrical furnace with a cylindrical vanadium-foil heating element of 22, 30 or 40 mm diameter around the sample cylinder allows investigations on powders and liquids from room temperature up to 1300 °C without significant background contributions from the sample environment.

With this instrument many time-resolved diffraction experiments have been performed. Walton et al. (2001) studied the hydrothermal crystallization of barium titanate, $BaTiO_3$. The formation of the ferroelectric ceramic could be investigated in real time and under genuine reaction conditions. A nucleation-growth model as proposed by Hancock and Sharp (1972), based on the expressions of Avrami (1939, 1940, 1941) and Erofeyev (1946), was able to simulate the growth curves of barium titanate. For further details on a description of nucleation and growth processes, see Lasaga (1998) and Kashchiev (2000). Fehr et al. (2003) and Walk-

Lauffer (2003) designed an autoclave cell to perform time-resolved neutron diffraction experiments on dynamic processes during hydrothermal reactions in the presence of a (deuterated) hydrous fluid as they occur in the synthesis of aerated concrete. They investigated the influence of different additives like anhydrite or potassium sulfate on the formation of 1.13 nm tobermorite from portlandite and quartz at 190 °C and saturation pressure. The reaction time was set to about 6 hours and the reaction product consisted of tobermorite, semi-crystalline calcium-silicate-hydrate C-S-H(I) and quartz. Tobermorite forms at the expense of portlandite and quartz and by the reaction of semi-crystalline calcium-silicate-hydrate C-S-H(I) with quartz. The reaction progress α is inversely proportional to the remaining amount of portlandite or quartz, and its evolution expressed as a product of a function of α and a kinetic constant k (Bray and Redfern 1999).

In situ neutron diffraction traced the reaction mechanism during the self-propagating high-temperature synthesis (SHS) of Ti_3SiC_2 and related ceramics from furnace ignited stoichiometric Ti/SiC/C mixtures (Riley et al. 2002, 2006). The diffraction patterns indicate five stages, visible in Figure 3: (1) pre-heating of the reactants, (2) the $\alpha \rightarrow \beta$ phase transformation in Ti, (3) pre-ignition reactions, (4) the formation of a single solid intermediate phase in less than 0.9 s and (5) the rapid nucleation and growth of the product phase Ti_3SiC_2. The $\alpha \rightarrow \beta$ phase transformation in Ti is a necessary precursor to the reaction as is the subsequent reaction of Ti and C just before SHS ignition. This latter process is exothermic and provides the extra heat required for sustained SHS to occur. No amorphous contribution to the diffraction patterns from a liquid phase was detected and as such, it is unlikely that a liquid phase plays an important role in this SHS reaction. The intermediate phase is believed to be a solid solution of Si in TiC such that the overall stoichiometry is approximately 3Ti:1Si:2C. Lattice parameters and known thermal expansion data were used to estimate the ignition temperature as 901 ± 8 °C (confirmed by the $\alpha \rightarrow \beta$ phase transformation in Ti) and the combustion temperature as 2320 ± 50 °C. In further experiments, the data acquisition time could be reduced to 300 ms with a dead time of 40 ms between two acquisitions.

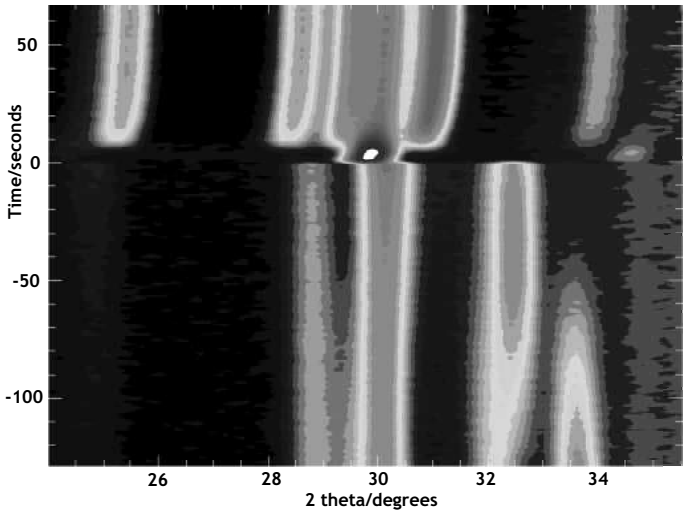

Figure 3. Contour plot of an angular range of 12° in 2θ during 200 s of the SHS of Ti_3SiC_2, representing about 220 diffraction patterns. 100 s before ignition ($t = 0$) the $\alpha \rightarrow \beta$ phase transition of Ti occurs (peaks at 32 and 34°). 30 s before ignition β-Ti is partially consumed to form TiC (peak at 30°). During the ignition (< 0.5 s), a solid solution of Si in TiC is formed. 2 s later, the intermediate product starts to decompose to Ti_3SiC_2 with a time constant of 5 s.

New electronic detectors developed at ILL permit much larger areas to be covered with two-dimensional PSDs. Hewat (2006) designed a new Diffractometer for Rapid ACquisition with Ultra-Large Area detector (DRACULA), to collect a 5 times larger solid angle than now possible with D20. In this it will approach the coverage of instruments at pulsed neutron sources. The advantage of using a reactor rather than a pulsed source is still that the time averaged flux on the sample can be an order of magnitude greater. DRACULA will become the fastest machine to study fast solid state reactions, with times slices of less than 100 ms.

Of course there are other facilities to perform time-resolved neutron diffraction studies. Time-resolved neutron diffraction is performed routinely on instruments such as GEM at ISIS (Williams et al. 1998; Radaelli et al. 2003; Hannon 2005) and HIPPO at LANSCE, though data acquisition times are considerably slower than with D20. PowGen3 under construction at SNS will set new standards for high-intensity TOF-diffraction with considerable promise for time-resolved investigations (Hodges 2004).

SAMPLE ENVIRONMENT

In almost all cases scientifically relevant time-resolved studies need to be performed at non-ambient temperatures and/or pressures. Often they need in addition a close control of the chemical activity of the involved species by adjusting the partial pressures of the gaseous constituents or surrounding atmospheres. In many cases these conditions need some modifications to standard equipment available at neutron scattering centers or even the development of purpose-built devices. It is beyond the scope of this review to give a full account of the sample environment options for neutron diffraction and it is impossible to give details on those purpose-built devices. Rather, we refer to the examples given further below to illustrate the preparations needed to do time-resolved studies. What should be said, however, is that complicated sample environments are usually more easily adapted to neutron scattering than to X-ray diffraction. General consideration for neutron scattering sample environments can be found in literature. Concerning high temperatures and high pressures very useful information is given in Part III of Reviews in Mineralogy and Geochemistry Vol. 41 (Peterson and Yang 2001). Fei and Wang (2001) focus on the state of art in synchrotron powder diffraction, but some of the large volumes presses, e.g., the so-called Paris-Edinburgh press (Besson et al. 1992), using developments of a toroidal high pressure device by Khvostantsev et al. in the 1970's, reviewed in Khvostantsev et al. (2004), found widespread application in time-of-flight and constant wavelength neutron diffraction (Parise 2006b, this volume). The current state of gas pressure cells used for some of the examples given below has been reviewed in a special issue of the proceedings of an International Workshop on Medium Pressure Advances for Neutron Scattering (Kuhs et al. 2005). A new design of a gas pressure cell combined with a closed-cycle helium cryostat is described by Lokshin and Zhao (2005).

Electrical furnaces with cylindrical heating elements of vanadium- or niobium-foil and concentric heat shields of the same material around the sample cylinder allow investigations on powders and liquids from room temperature up to about 1900 K (Bletry et al. 1984). Vanadium is preferred for its low background contribution in terms of parasitic Bragg peaks resulting from its low coherent scattering cross section, whilst niobium permits to obtain higher temperatures. Even higher temperatures, up to 2300 K, can be obtained with so-called mirror furnaces (Lorenz et al. 1993). Holland-Moritz et al. (2005) developed an electromagnetic levitation furnace, which allows container-less investigations, e.g., on super-cooled metallic melts.

To achieve low temperatures, the so-called *Orange Cryostat* has been developed at ILL in 1975. Cryogenic liquids such as nitrogen or helium do not interact with the neutron beam, and the only metal, the neutron beam is passing through, is aluminum or vanadium. The cryostat

has a liquid nitrogen jacket, its liquid helium flow is controlled with a cold valve, it shows no interference between the calorimeter and the flow of the cryogenic liquid, and the sample is in thermal equilibrium with an exchange gas. The standard orange cryostat has a sample access of 49 mm diameter and is operational in a temperature range from 1.4 to 320 K. At D20, the calorimeter is of a smaller diameter of 25 mm and made of vanadium to allow for cleaner powder diffraction patterns.

The so-called cryofurnace based upon the Orange Cryostat design has been developed at ILL in 1983. It allows extending the accessible temperature range up to 600 K by avoiding indium seals at the calorimeter. Lower temperatures can be achieved with dilution inserts. Today, due to the high price of helium price and for ease of operation, closed-cycle refrigerators more and more replace Orange Cryostats, apart from very low temperature applications.

Various kinds of chemical reactors have been developed mostly for particular experiments, e.g., hydrothermal autoclaves either receiving the heating from an existing furnace (Fehr et al. 2003; Walk-Lauffer 2003) or equipped with its own heating system (Walton et al. 1999). Latroche et al. (2002) developed dedicated electrochemical cells.

For time-resolved investigations it is often crucial to reach the wanted thermodynamic conditions in the shortest possible time and to control them closely once the reaction is started. Environments of high inertia, often linked to high accuracy, can limit considerably the time-resolution and complicate the data treatment. In any case, it must be possible to change the thermodynamic conditions on beam, which is a particular challenge for time-resolved high pressure studies using mechanical clamps.

EXAMPLES

Water ices and gas hydrates are important materials on earth, the solar system and beyond. Hydrogen is the most common element in the Universe. Ice is widespread in many the outer smaller planets, the moons of Jupiter and Saturn or the nuclei of comets (Schmitt et al. 1998; Max 2003; Yershov 2004; Max et al. 2006). These compounds represent traditional fields of investigation for neutron diffraction. Neutrons allow to obtain details on the hydrogen positions and to establish the degree of proton ordering which may vary as a function of pressure and temperature. Neutrons also have advantages in high pressure studies; the medium pressure range in particular was object of numerous structural studies by neutron diffraction. The complex phase diagram of water is shown in Figure 4 exhibiting stable and metastable phases, some of which have no regime of thermodynamic stability at all (Petrenko and Whitworth 1999). While the melting curves are fairly well known, most of the phase boundaries between the solid phases are not well established, largely due to a considerable hysteresis, in particular at low temperatures. Even less is known in terms of the kinetics of the phase transitions between the different forms of ice and the reactions of various gases with ice leading to so-called "filled" ices (in which gas molecules enter and leave without breaking H-bonds) or to clathrate hydrates with encaged gas molecules (Kuhs 2004). Time-resolved neutron diffraction provides an excellent way to gain deeper insight into the transformation mechanisms on both topological or proton ordering transitions in ice as well as the uptake/release reactions with various gases and the underlying rate limiting processes.

The following three examples for time-resolved studies concentrate on the transformation kinetics of ices and gas hydrates. They include a number of experimental details, which should highlight some of the necessities and technical constraints typical for time-resolved work; some limitations will also be discussed. Each example closes with some more generally valid remarks concerning time-resolved work. For any more detailed information on the scientific implications of the results the reader is referred to the original literature cited.

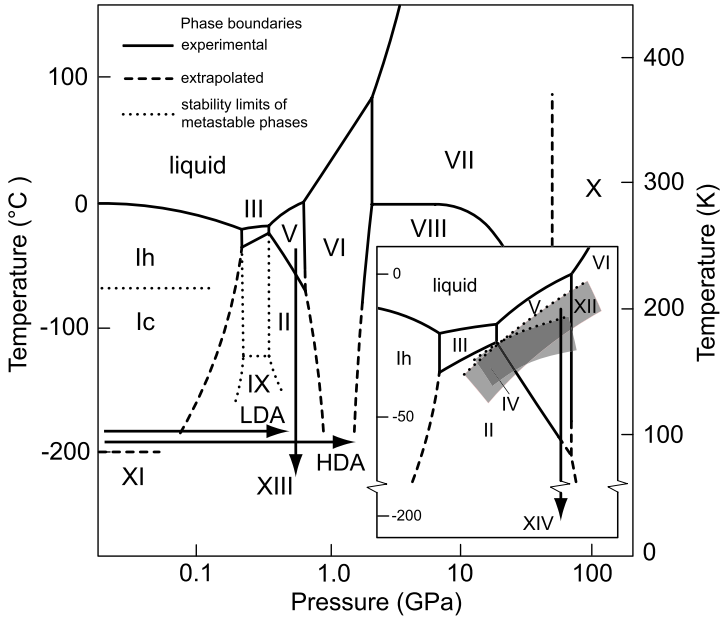

Figure 4. Phase diagram of water and water ices including some recently discovered stable and metastable forms (Lobban et al. 1998; Salzmann et al 2006). Arrows indicate the typical preparation paths (low-temperature pressurization or controlled cooling) for LDA; HAD, ice XIII and XIV. The insert shows an enlarged part of the medium pressure range where several forms of ice co-exist.

Kinetics of the high–density to low–density amorphous ice transition

Background. At least two different disordered states of water ice at low temperatures are known (Mishima et al. 1984), a *high-density amorphous* (HDA) ($\rho_{H_2O} \approx 1.17$ gcm^{-3}) and a *low-density amorphous* ice (LDA) state ($\rho_{H_2O} \approx 0.93$ gcm^{-3}). This phenomenon is known as *polyamorphism* (Mishima et al. 1985; Bosio et al. 1986; Floriano et al. 1986; Bellissent-Funel et al. 1987; Bizid et al. 1987; Mishima and Stanley 1998). Both states transform into each other when heating the sample above $T \approx 100$ K at ambient pressure (HDA $\rightarrow$ LDA) or when compressing the sample above $P \approx 1$ GPa at $T < 160$ K (LDA $\rightarrow$ HDA) (Mishima et al. 1991; Mishima 1994, 1996). Calorimetric experiments revealed the release of latent heat at the HDA $\rightarrow$ LDA transformation (Handa 1986b), indicating a first-order phase transition. On the other hand, LDA shows upon heating an onset of an endothermic transition before it crystallizes exothermally to cubic ice. This has been interpreted as a glass transition of LDA with $T_g \approx 140$ K (Johari et al. 1987; Handa and Klug 1988; Johari et al. 1991; Johari 1995), whilst Velikov et al. (2001) revised this value to $T_g \approx 165$ K.

Although the described experimental results on HDA and LDA are compatible with a first-order transition between two supercooled liquid states and experimental results are often referred to as due to a first-order phase transition, some experimental results contradict the idea of HDA and LDA being supercooled liquids. It lead to the discovery of a third disordered modification, a *very high density amorphous* ice (vHDA) with $\rho_{H_2O} \approx 1.25$ gcm^{-3} (Loerting et al. 2001).

Several distinct models are discussed to account for the existence and properties of the amorphous phases. Poole et al. (1994) introduced a model, which brought the proposed second critical point ($T_c \approx 220$ K, $P_c \approx 100$ MPa) with an emerging line of first-order transition

towards lower temperatures (Poole et al. 1992) and the scenario of a retracing of the vapor-liquid spinodal in the supercooled region of water's phase diagram (Speedy 1982a,b; Sastry et al. 1993) together. In contrast to this model, in which intermediate states of the transition should reflect the superposed properties of the involved phases, a singularity-free model (Stanley and Teixeira 1980; Geiger and Stanley 1982) implies a continuous change of observables. The *in situ* neutron diffraction sampling of the static structure factor gave Koza et al. (2003) the opportunity of extracting information on the kinetics of the transformation and on the properties of the intermediate states, i.e., to distinguish between continuous variation of the amorphous structure and a superposition of the HDA and LDA structures in the course of the transformation.

Experimental. All HDA samples were prepared by slow compression of deuterated crystalline ice Ih ($V \approx 2.5$ ml) in a piston–cylinder apparatus at $T = 77$ K up to $P \approx 1.7$ GPa (Koza et al. 1999, 2000). After HDA had been formed the pressure was released and the sample retrieved from the pressure device under liquid nitrogen and transferred in cylindrical sample containers into an Orange Cryostat at $T = 77$ K. The evaporation of nitrogen from the sample containers was carried out at $T = 78$–79 K and controlled via the scattering signal of the samples. For each sample, the static structure factor of HDA and, after the *in situ* measurements, of LDA was determined at $T = 77$ and 127 K, respectively. At these conditions both amorphous states could be well reproduced.

Two different types of thermal treatment were applied to the samples. First, measurements were performed on samples that were heated directly from the HDA state to the nominal temperature T. A second set of experiments was performed on samples that had been pre-annealed at a temperature T_{an} and heated subsequently to the nominal T with $77\ \mathrm{K} < T_{an} < T < 127$ K. The data collection started in all cases before the heat treatment was applied. This allowed us to monitor the transformation process continuously. Data were collected on the diffractometers D4 (incident neutron wavelength $\lambda = 0.7$Å) and D20 ($\lambda = 1.3$ and 2.4 Å) and the time-of-flight spectrometer IN6 ($\lambda = 4.1$ Å) at ILL. The raw data are corrected for different detector efficiencies and empty container scattering. To compare the energy-resolved time-of-flight data (IN6) with those from the diffraction instruments (D4 and D20) an energy integration is performed as $S(2\theta) = S(2\theta,\ t = 0) = S(2\theta,\ \omega)\ d\omega$. All data sets are finally converted via the mapping $S(2\theta) \rightarrow S(Q)$. Figure 5 shows the obtained $S(Q)$ of HDA and LDA as measured on D20.

Analysis. The data analysis is done on the *relative* changes of the structure factors observed while the sample passes from the HDA into the LDA state. The difference profile obtained from subsequent data sets with respect to a reference $S(Q)$, e.g., the $S(Q)$ of LDA, provides a convenient mathematical expression for monitoring these changes (Schober et al. 1998). $S(Q;\mathrm{HDA})$ and $S(Q;\mathrm{LDA})$ are taken as the static structure factors of HDA and LDA at 77 K and at 127 K, respectively. $I(t,T)$ is one for pure HDA and zero for pure LDA.

$$I(t,T) = \frac{\int_{Q_1}^{Q_2} S(Q;\mathrm{LDA}) - S(Q;t,T)\,dQ}{\int_{Q_1}^{Q_2} S(Q;\mathrm{LDA}) - S(Q;\mathrm{HDA})\,dQ} \tag{1}$$

In a pure first-order transition the structure factors of the intermediate states can be expressed as a superposition of those of the initial and the final phases. In that case, $I(t,T)$ stands for the fraction of initial material HDA still present at time t and temperature T. For practical reasons, the integration limits have been chosen to $Q_1 = 1$ Å^{-1} and $Q_2 = 2.65$ Å^{-1}, a range covered by the whole series of experiments on different instruments (mainly D20, but also D4 and IN6 for some temperatures). Figure 6 shows $I(t,T)$ as determined from an experiment at D20 at two different temperatures.

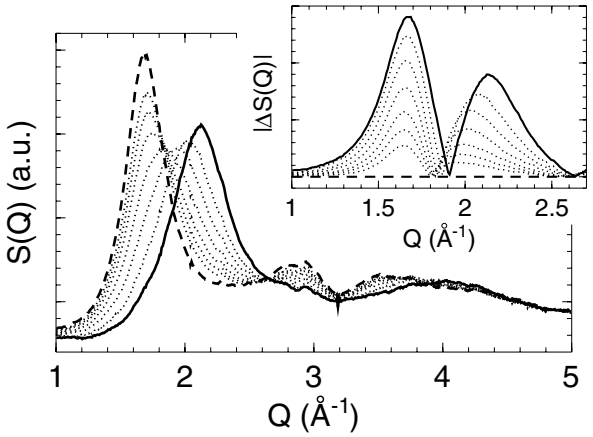

Figure 5. Evolution of the static structure factor $S(Q)$ during the transition from HDA (solid) to LDA (dashed) ice. Intermediate data (dotted) are selected from an *in situ* measurement of the transition performed at D20 at $T = 110$ K. The inset shows the difference of $S(Q;T)$ at corresponding conversion stages with respect to $S(Q;\mathrm{LDA})$: $|\Delta S(Q)| = |S(Q;\mathrm{LDA}) - S(Q;t)$ [Used by permission of Institute of Physics Publishing, from Koza et al. (2003), *Journal of Physics: Condensed Matter*, Vol 15, Fig. 1, p. 323].

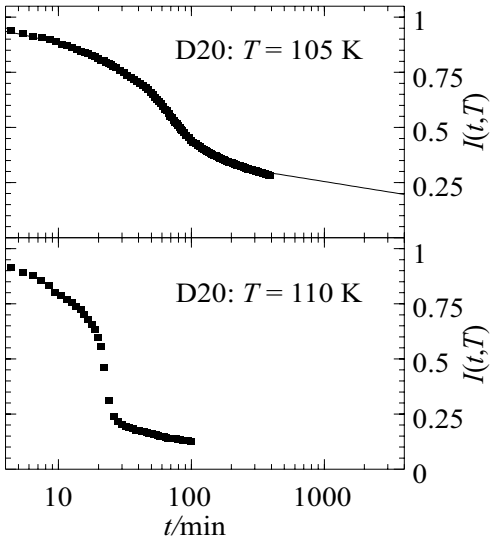

Figure 6. Temperature dependence of the transformation kinetics of HDA to LDA. The sigmoid-shape of $I(t,T)$ can be represented by superposition of the logarithmic HDA annealing and an *Avrami-Kolmogorov* behavior, reminiscent of a first-order transition. Such a fit to the data corresponds to the solid line in the graph for data at 105 K [after Koza et al. (2003)].

The time dependence of $I(t,T)$ could be fitted with a superposition of a logarithmic response and an *Avrami-Kolmogorov* equation (AKE) (Avrami 1939,1940,1941; Kolmogorov 1937), as described by Doremus (1985).

$$I(t,T) = (1-C) + C\exp\left[-\left(\frac{t}{\tau_0(T)}\right)^n\right] + B\ln(t) \qquad (2)$$

The logarithmic relaxation—the left part of Equation (2) (B is increasing with temperature)—is observed in other amorphous materials as well (Primak 1975; Grimsditch 1986; Tsiok et al. 1998) and is expected for the relaxation of materials with double-well potentials (Karpov and Grimsditch 1993) and from simulations of aging of liquids (Sciortino and Tartaglia 2001).

However, no additional transformation stages beyond the logarithmic relaxation have yet been revealed. The AKE behavior above 103 K is an additional transformation process

consistent with a first-order transition, as it indicates nucleation and growth of a homogeneous low-density phase within a homogeneous high-density matrix. The exponent n in Equation (2) refines to $n \approx 1.5$, as expected for diffusion-controlled transitions with short nucleation times and isotropic growth (Doremus 1985; see also Pradell et al. 1998).

Apart from the fact that a well annealed HDA state does exist, after logarithmic relaxation, which will transform to LDA following a pure AKE behavior, the final state of this transition does not coincide with the LDA state one obtains after annealing at $T = 127$ K. The results show three states of the HDA-LDA transformation, an annealing stage of HDA, then the transition which seems to be a first order transition with coexistence of HDA and LDA and not a continuous change from HDA to LDA (to check this, the total $S(Q)$ must be a linear combination of the individual $S(Q)$ for each phase). Once the LDA is formed, it still anneals in a third stage, annealed LDA. To distinguish the later, the un-annealed LDA is hereafter called LDA′.

The activation energy ΔE results from exploiting the Arrhenius Equation (3); Figure 7 shows the corresponding Arrhenius plot.

$$\tau(T) = \tau_\infty \exp\left(\frac{\Delta E}{RT}\right) \tag{3}$$

ΔE has been determined to $\Delta E = (33\pm2)$ kJ·mol^{-1} and $\tau_\infty \approx 10^{-13\pm1}$ s which is a physically reasonable attempt time for crossing the energy barrier ΔE.

Further investigations. Koza et al. (2005) showed, that HDA ices obtained from compression of crystalline ice Ih or from vHDA ice as an intermediate stage (hereafter called HDA′) of its transition into LDA′ ice seem to be identical in terms of $S(Q)$ obtained from neutron diffraction at D20. The kinetics of the vHDA to LDA′ transition at different temperatures is shown in Figure 8. During the annealing of vHDA, $S(Q)$ increases below $Q \approx 0.6$ Å. This small angle scattering signal reaches its maximum (the state of strongest heterogeneity, SSH) briefly after having passed the state of HDA′ (HDA, obtained from ice Ih, shows the same signal level at low Q), before dropping drastically in the apparent first-order transition of HDA′ to LDA′. The enhanced low-Q signal coincides with the behavior

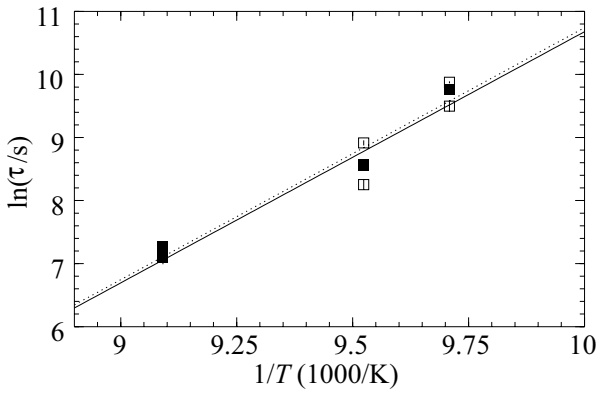

Figure 7. Arrhenius plot of time constants for the transformation of HDA to LDA calculated by different techniques – (open squares) determined with Equation (1) and (full squares) calculated from position of maximum in $S(Q)$. Lines correspond to linear fits, estimating the fit uncertainty by the deviation of all data points (solid line) and by taking the experimental error and temperature step width into account (dashed line) [Used by permission of Institute of Physics Publishing, from Koza et al. (2003), *Journal of Physics: Condensed Matter*, Vol 15, Fig. 7, p. 329].

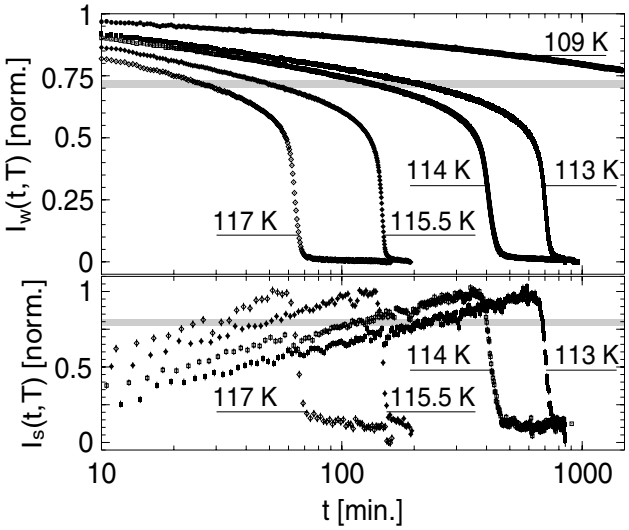

Figure 8. Kinetics of the vHDA into LDA′ transition, nominal temperatures given in the figure. The gray shaded area indicates the position of HDA′ and, respectively, HDA in the plot. The kinetics of the transient intensity at low-Q is shown below. Equation (1) defines I_w and I_s with $Q_1 = 0.6$ Å^{-1} and $Q_2 = 2.75$ Å^{-1} for wide-angle data (I_w), respectively $Q_1 = 0.35$ Å^{-1} and $Q_2 = 0.55$ Å^{-1} for small-angle data (I_s). [Reprinted figure with permission from Koza et al. (2005), *Physical Review Letters*, Vol. 94, Fig. 4, p. 125506-3. *http://link.aps.org/abstract/PRL/v94/e125506*. Copyright 2005 by the American Physical Society.].

of the wide-angle $S(Q)$, its Fourier transform $D(r)$ shows in contrast to vHDA and LDA′ no oscillations beyond $r > 10$ Å, indicating a reduction of spatial correlations. Thus, HDA and HDA′ are heterogeneous structures. Although they look the same, the kinetics of their transition to LDA′ seems to be different. However, the fact that the transitions shown in Figure 8 are so fast and hard to fit with the Avrami-Kolmogorov expression, Equation (2), is also due to the fact that the speed of the transition at temperatures above $T \approx 110$ K is so high, that the evacuation of latent heat from the exothermic reaction cannot be assured, isothermal conditions are no longer fulfilled, and the exponent n in Equation (2) increases artificially—if a fit is possible at all—as the non-evacuated heat accelerates the transition due to a locally higher temperature.

In a recent series of experiments, Koza et al. (2006) combined neutron powder diffraction and small angle neutron scattering (SANS) to show that there are only two homogeneous disordered ice structures, vHDA and LDA. They come to the conclusion that the HDA state does not constitute any particular state of the amorphous water network, while Loertig et al. (2006) interpret their results otherwise. It is formed due to the preparation conditions, which determine the degree of heterogeneity. This can be quantified by SANS, using the DBM model proposed by Debye and Bueche (1949) for a mixture of two statistically distributed phases. If both phases present 50% of the total, an average domain size D results easily from twice the correlation length. This is exactly the situation for the SSH, where domain sizes from 11 to 13 Å have been determined for all investigated samples. The transformation speed increases systematically with a sample being of increasing heterogeneity. The precise reason for this is still subject to scientific discussion; possible models considered are those given by Adam and Gibbs (1965) or by Tanaka (2000).

In summary, kinetic studies of transitions between amorphous ices provided key information to understand the complex phenomenon of polyamorphism and they will be

necessary in the future to quantify the nature of the heterogeneous states. This example also shows that a single experimental technique often is insufficient to get a complete understanding of the involved processes; here SANS proved to be a very powerful addition and, indeed, SANS is very apt to see the onset of time-dependent transformations better than wide angle diffraction, given that a scattering contrast develops (see Cole et al. 2006, this volume; Radlinski 2006, this volume; Wilding and Benmore 2006, this volume).

Synchrotron X-ray diffraction presents an alternative technique to neutron diffraction in this context, able to cover a wider Q-range at once and thus combining wide-angle- and small-angle-scattering. Also, the incoherent scattering from protons or deuterons is no longer a problem with X-ray diffraction, and the insensitivity to scattering from protons and deuterons is even an advantage in this particular case, as this polyamorphism is sufficiently expressed by the oxygen positions alone. Nevertheless, drawbacks of X-ray scattering are the low scattered intensity from light atoms and thus relatively long counting times and at the same time the enormous heat-load from the incident X-ray beam on the sample. The latter makes it very difficult, if not impossible, to keep the temperature stable and to have the sample in a thermodynamically well defined and stable state. In particular kinetic experiments suffer from this a lot and neutrons appear still as a good first choice.

Gas hydrate formation kinetics

Background. Gas hydrates are non-stoichiometric inclusion compounds encaging small, usually apolar guest molecules in a host-framework of hydrogen bonded water molecules. They exist as a stable solid phase at high gas pressures and/or low temperatures. Two main crystallographic structures of gas hydrates, the von Stackelberg cubic structure I and II (von Stackelberg and Müller 1954), are distinguished (Fig. 9) both consisting of two types of cavities, small and large cages, that can be occupied by the guest molecules to various degrees in a non-stoichiometric manner. It is generally assumed that the encaged gas molecules cannot exchange with the environment after formation. Rather, the guest molecules have to be built into the crystal structure during the growth process according to their chemical activity at the reaction site.

Since the 1950's, a large number of gas hydrate systems have been studied . The geologically and economically most important methane-water phase diagram is shown in Figure 10. Despite some 6000 publications, several physico-chemical properties of gas hydrates as well as their

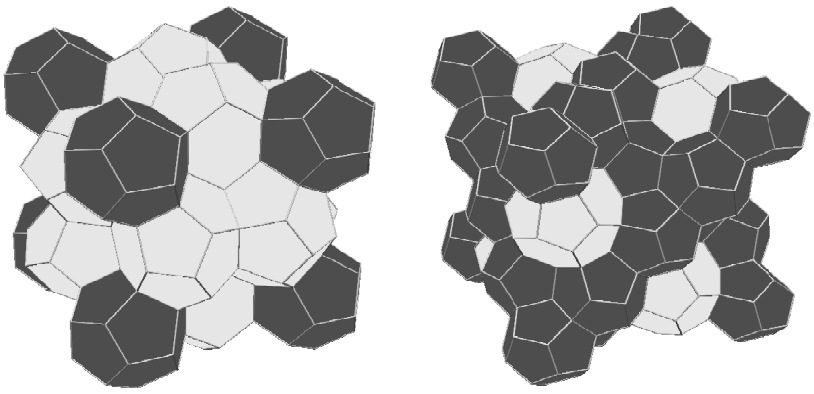

Figure 9. Schematic representation of clathrate hydrate structures of type I (left) and type II (right). Only the polyhedrons formed by oxygen are displayed. One unit cell is shown in each case. The smaller 5^{12} pentagon-dodecahedral cages (2 per unit cell, bcc packed, in type I; 16 per unit cell, ccp in type II) are drawn in dark grey, the larger $5^{12}6^2$14-faced polyhedrons (6 per unit cell in type I) and $5^{12}6^4$ 16-faced polyhedrons (8 per unit cell in type II) are drawn in light grey.

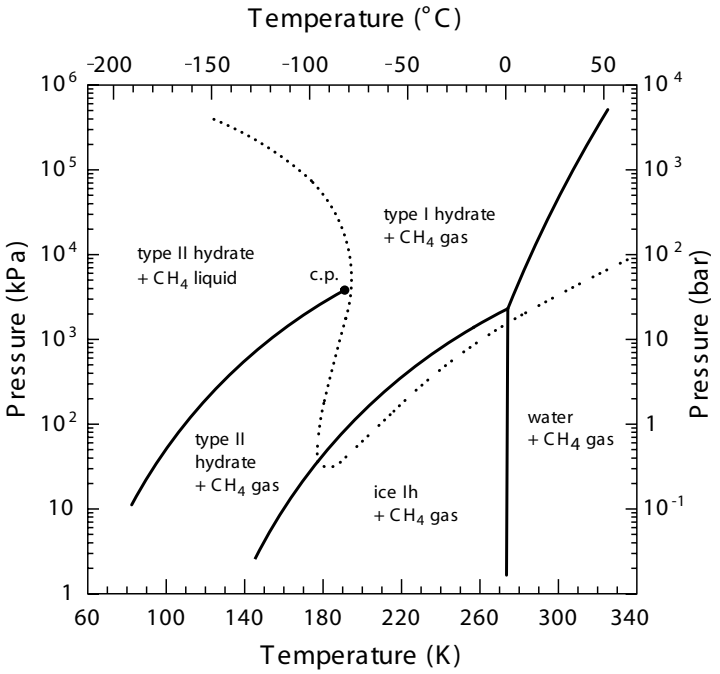

Figure 10. Phase diagram of the system water-methane. Bold lines give the established phase boundaries of water, ice, methane hydrate as well as liquid and gaseous methane with its critical point (c.p.). The dotted line represents a calculated phase boundary for structure I and structure II methane hydrate as calculated by Lundgaard and Mollerup (1992); the experimental separation line between structure I and II methane hydrate is not established.

formation and decomposition kinetics are neither well known nor properly understood, though they are of primary importance for a number of reasons. With traces of water in gas and oil pipelines operated at gas pressures well within the hydrate stability field, gas hydrates can form leading to a complete blockage. Likewise, the kinetics of CH_4-hydrate formation and decomposition is of major significance in geological settings, for our understanding of the role of methane gas in climate change, for a possible use of natural gas hydrate deposits as a future source of energy or simply for a more economic transport and storage of gas. CO_2 clathrate hydrates could also be a possible form of sequestering CO_2 into geological formations to reduce global warming. They may also play a major role for a number of terra-forming processes on Mars (Kargel 2004). Not much is known on the formation kinetics of CO_2 hydrates under Martian conditions and it is not certain that they form at the surface in any substantial amount due to the diurnal or annual temperature cycles. Our neutron diffraction work was intended to establish the formation and decomposition kinetics and in this way build a solid physico-chemical basis for the cases listed above.

In the Martian context, the most relevant formation process is the reaction of ice Ih with CO_2 gas to hydrate. A strong dependence of the transformation rates on the surface area of the gas-ice contact was demonstrated by Barrer and Edge (1967). Later, Hwang et al. (1990) studied the methane-hydrate growth on ice as a heterogeneous interfacial phenomenon and measured the clathrate formation rates during ice melting at different gas pressures. Sloan and Fleyfel (1991) discussed molecular mechanisms of the hydrate-crystal nucleation on ice surface, emphasizing the role of the quasi-liquid-layer (QLL) on ice. Takeya et al. (2000) made in situ

observations of the CO_2-hydrate growth from ice powder for various thermodynamic conditions using laboratory X-ray diffraction. They distinguished the initial ice-surface coverage stage and a subsequent stage which was assumed to be controlled by gas and water diffusion through the hydrate shells surrounding the ice grains. The process was modeled following Hondoh and Uchida (1992) and Salamatin et al. (1998) in a single ice particle approximation. The respective activation energies of the ice-to-hydrate conversion were estimated as 0.2 and 0.4 eV (4.6 and 9.2 kcal/mol). The first in situ neutron diffraction experiments on kinetics of the clathrate formation from ice powders were presented by Henning et al. (2000). They studied the CO_2-hydrate growth on D_2O ice Ih, using the high intensity powder diffractometer HIPD at IPNS for temperatures from 230 to 263 K at a gas pressure of approximately 6.2 MPa. The starting material was crushed and sieved ice with unknown but most likely irregular shape of the grains. To interpret their results, the authors applied a simplified diffusion model of the flat hydrate-layer growth developed for the hydration of concrete grains. The activation energy of 6.5 kcal/mol was determined for the later stage of the hydrate formation process. This work has been continued by Wang et al. (2002) to study the kinetics of CH_4-hydrate formation on deuterated ice particles using neutrons. Their more sophisticated shrinking-ice-core model can actually be reduced to the diffusion model of Takeya et al. (2000, 2001). A higher activation energy of 14.7 kcal/mol was deduced for the methane hydrate growth on ice. Based on findings by Mizuno and Hanafusa (1987), the authors suggested that the quasi-liquid layer of water molecules at the ice-hydrate interface may play a key role in the (diffusive) gas and water redistribution although a definite proof could not be given. For further details on shrinking core models the reader is referred to detailed accounts by Froment and Bischoff (1990) and Levenspiel (1999).

In accordance with numerous experimental observations (Uchida et al. 1992, 1994; Stern et al. 1998; Henning et al. 2000; Kuhs et al. 2000; Takeya et al. 2000; Staykova et al. 2003), a thin gas-hydrate film rapidly spreads over the ice surface at the initial stage (stage I) of the ice-to-hydrate conversion. Subsequently, the only possibility to maintain the clathration reaction is the transport of gas molecules through the intervening hydrate layer to the ice-hydrate interface and/or of water molecules from the ice core to the outer hydrate-gas interface. As mentioned above, a diffusion-limited clathrate growth was assumed and simulated by Takeya et al. (2000), Henning et al. (2000), and Wang et al. (2002) on the basis of the shrinking-core models formulated for a single ice particle. However, in the case of porous gas hydrates, the gas and water mass transport through the hydrate layer becomes much easier, and the clathration reaction itself may be the rate-limiting step at a second stage of the hydrate formation that proceeds after the ice-grain coating. Certainly, we still can expect the onset of the further stage of the hydrate formation process completely or, at least, partly controlled by the gas and water diffusion through the hydrate phase, especially when a highly consolidated ice-hydrate structure develops with thick and dense hydrate shells surrounding ice cores. As a result, the hydrate-phase growth and expansion beyond the initial ice-grain boundaries into the sample voids and the corresponding reduction of the specific surface of the hydrate shells exposed to the ambient gas can be a principal factor which slows down the hydrate formation rates at the later stages of the clathration reaction, as predicted in Staykova et al. (2003) and confirmed in Kuhs et al. (2006). It should also be noted that in some cases a metastable formation of gas hydrates in a different structure (type I or type II) can be observed with a slow transformation into the stable phase (Halpern et al. 2001; Chazallon and Kuhs 2002; Staykova et al. 2003). The kinetics of a thermodynamically driven type I/ type II transition upon gas exchange has been studied using time-resolved neutron diffraction by Halpern et al. (2001).

Several studies were performed to quantitatively describe the formation process of CH_4 and CO_2 gas hydrates, both by in situ neutron diffraction on the high-flux diffractometer D20 of ILL as well as by in-house gas consumption experiments. While neutron experiments give unique access to the fast initial part of the clathration reaction, in-house gas consumption experiments are indispensable for the later, slower stages of the hydrate formation. Together with our kinetic

diffraction studies, *ex situ* FE-SEM (field-emission scanning electron microscopy) observations of the formation of gas hydrates proved to be very helpful to better understand the evolution the ice microstructure during the clathration reaction and to construct a phenomenological multi-stage model of the gas-hydrate growth from ice powders (Staykova et al. 2003).

Experimental. Here, we summarize our above-cited recent work in which we attempted to quantitatively describe all stages of the formation process of CH_4 and CO_2 gas hydrates as followed by in-situ neutron diffraction and gas consumption experiments, starting from a well characterized ice-powder of known structure, grain size, and specific surface area. The high gas pressure needed to form and investigate gas hydrates in situ makes neutron diffraction a prominent tool for their investigation as neutrons have no problem to penetrate through thick-walled gas pressure cells located in a cryostat. While neutron experiments give unique access to the fast initial part of the clathration reaction, in-house gas consumption experiments are indispensable for the later much slower stages of the hydrate formation due to beam-time limitations. These in-house experiments were calibrated using neutron and X-ray (synchrotron as well as laboratory) diffraction techniques; without such a calibration the determination of the absolute degree of transformation by gas consumption methods is bound with large errors.

Spherical D_2O ice Ih grains with a typical diameter of several tens μm were prepared using a spraying technique. In order to quantify the morphology of the starting material, a representative part of the sample was investigated by cryo-FE-SEM. The pictures obtained were used to estimate the size distribution of the ice spheres. Measurements on different batches showed that the size distribution of ice spheres sprayed with the same nozzle is well reproducible and has a lognormal shape. The mean radius has been determined as 27 μm at relative standard deviation of 0.8. Samples with a packing density of about 65-70% were placed in high strength auto-frettaged aluminum gas pressure cells (Kuhs et al. 2005). The sample temperature reading was obtained from a calibrated temperature sensor fixed to the pressure cell wall. The Al sample cans were inserted into the pressure cell, already fixed to the sample stick, and the Bridgman seal was closed. This filling-operation was performed with a small stream of gas applied to ensure a complete gas filling of the system. Subsequently, the pressure cell was inserted into the orange cryostat and the temperature was equilibrated at the chosen value. Then the wanted gas pressure was applied within a few seconds while data collection was started concomitantly. As the settling of the pressure takes a few seconds, there is a corresponding uncertainty of the start of the reaction. In the case presented here this is within the chosen time resolution of the instrumental set-up and did not present an additional limitation.

To observe the changes of the diffraction patterns during gas hydrate formation we used D20 at its highest intensity setting at a wavelength of $\lambda = 2.414$ Å. The reaction of gas (at constant applied pressure and temperature) with ice grains was followed over a period of typically 10 to 20 h. Data were collected with a time resolution of 30 s or 1 min for the initial fast reaction and with a resolution of 5 min for the slower later part of the reaction. In this way data of good statistical precision were obtained, suggesting that even time-slices of several seconds would deliver useful information. To all data an efficiency correction and a background subtraction were applied. Subsequently, the measurements were analyzed in an automated way with the use of the full-pattern Rietveld refinement program GSAS (Larson and van Dreele 1990) delivering quantitative information on the amount of gas hydrate formed as a function of time with an accuracy of about 0.1 %. A two-phase (ice Ih + gas hydrate) Rietveld fit of the powder diffraction pattern obtained for each time slice was performed (Fig. 11). Refined parameters were the lattice constants of ice Ih and gas hydrate, the phase fractions and five to six background parameters; scale factor and absorption coefficient were fixed. The atomic positions and displacement parameters for D_2O ice Ih and CH_4- or CO_2-hydrate phases were taken from Klapproth (2002) and Klapproth et al. (2003) and were also kept fixed as no changes were expected. The weight fraction of the gas hydrate phase α (mole fraction of ice converted to

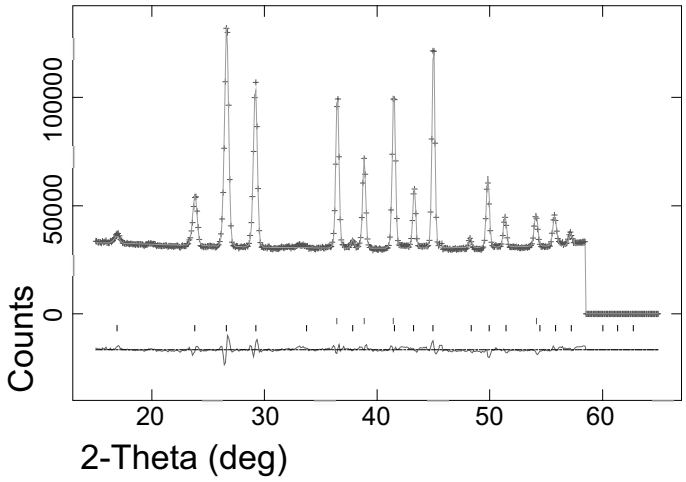

Figure 11. Low-angle part of a powder diffraction pattern obtained at a neutron wavelength of 2.414 Å of one time slice of a methane hydrate formation run at about 70% conversion at a temperature of 245 K with Rietveld-refinement result overlaid; crosses correspond to data points with a continuous line representing the calculated profile; top sequence of tick-marks represent ice Ih peak positions, bottom sequence to structure I hydrate peak positions; the bottom continuous line gives the difference between observed and calculated data points. The excluded region at angles > 59° correspond to a Bragg reflection of the Al pressure cell.

the gas hydrate) was extracted from the refinement for each time slice and plotted as a function of time (Fig. 12). An excellent statistical precision of the refined α's of 0.1% was obtained, which is hardly achieved by any other method. Moreover, also the accuracy of the obtained α's is distinctly superior to e.g., our gas consumption runs as the amount of formed gas hydrate is determined rather directly from a Rietveld refinement. Admittedly, what helped here was the fact that the hydrate formed is free of any texture and consists of an ideal powder with a typical crystallite size of a few μm to a few tens of μm. If the materials involved in the transformation are less ideal powders, this favorable situation for the determination of a reaction degree may deteriorate considerably.

In order to extend the time covered by the neutron runs with their inherent high data quality so-called "intermittent" experimental runs were performed which lasted 5-6 days (Kuhs et al. 2006). In both cases, the clathration reaction was started in the orange cryostat on the diffractometer and was tracked by neutron diffraction for about 20 h. Then the data acquisition was interrupted and the gas-pressure cell (stick) with the sample was moved to a separate low temperature bath where the reaction was continued out of the beam for a few days under identical conditions. During this time other users could perform their experiments on D20. Then each stick was placed back into the orange cryostat to measure the current reaction degree two more times—in the middle and at the end of the observation period.

Analysis. A detailed discussion of the models for analyzing the diffraction data is not given here; the interested reader is referred to the original publications (Staykova et al. 2003; Genov et al. 2004; Kuhs et al. 2006). It is sufficient to say that the starting material is reasonably described as a random dense packing of ice spheres as evidenced by cryo scanning electron microscopy. The neutron data were used to establish and refine a multi-stage model of the gas hydrate growth from ice Ih (Salamatin and Kuhs 2002) considering the influence of temperature and gas fugacity (which is related to the mechanical gas pressure) and using approximations for random dense packings introduced by Arzt (1982). A relatively short initial

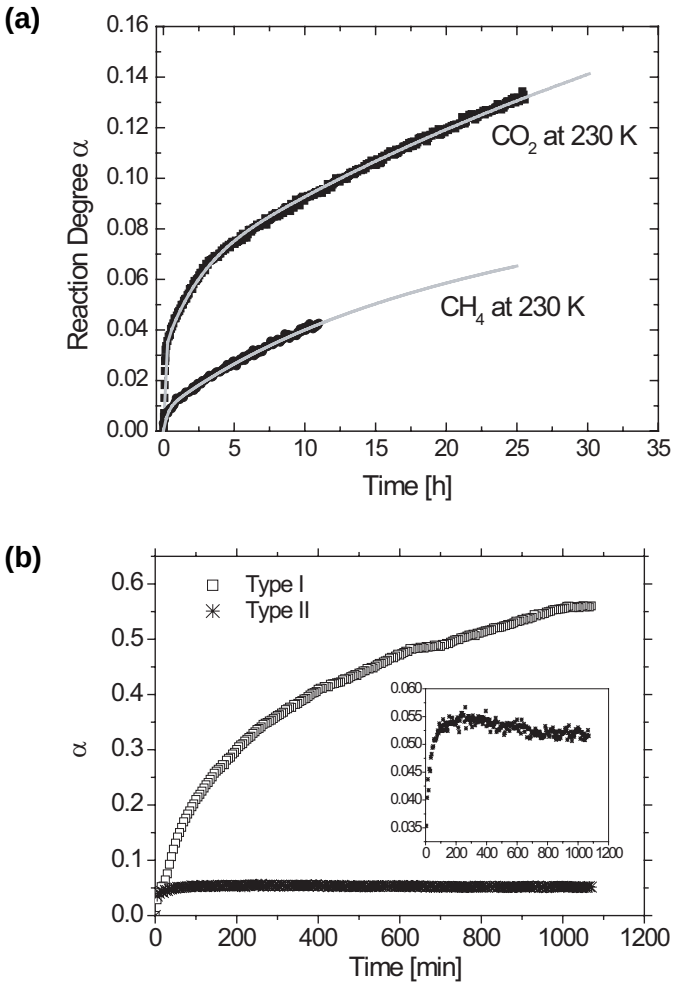

Figure 12. (a) Temperature dependency of the weight fraction of the transformed hydrate phase (reaction degree α): experimental points by symbols, fitted shrinking core model shown as gray curve [from Genov et al. (2004)]. (b) Simultaneous formation of a type I and type II structure of CO_2 hydrate. The insert shows the fraction of the metastable phase II, which after initial formation slowly back transforms into the stable structure I phase. Diffraction is the best tool to study the kinetics of this transformation. [Used by permission of Kluwer, from Kuhs (2004), in: High Pressure Crystallography, A. Katrusiak and P. McMillan (eds.), Fig. 7, p. 484]

stage I of hydrate film formation on the ice surface was distinguished followed by a stage II which generally includes two steps (sub-stages) presented by the clathration reaction at the ice-hydrate and gas-hydrate interfaces and by the diffusive gas and water transport through the hydrate shells surrounding shrinking ice cores. While the initial model was assuming monodispersity of the ice spheres, recently by generalizing Arzt's (1982) results an improved model for the hydrate growth in a polydisperse ensemble of randomly packed ice spheres was developed (Kuhs et al. 2006). This is of particular importance for the later stages of the gas hydrate formation. The difference in size of spherical ice particles in polydisperse samples results in different rates of their conversion to hydrates and part of the larger-size fraction

becomes frequently isolated and switched out of the reaction. This additionally slows down the ice-to-hydrate conversion and stops the hydrate growth in the sample before the complete transformation is achieved. It could be shown that stage II, being dominated by the diffusive gas/water transport through the growing hydrate layer, still may be noticeably influenced by the interfacial clathration reaction. The principal kinetic parameters, reaction rate constant k_R and permeation (mass-transfer) coefficient D were inferred from the neutron diffraction and gas consumption data. The respective activation energies obtained from a the least-squares Arrhenius approximation are $Q_R \approx 92.8$ kJ/mol and $Q_D \approx 52.1$ kJ/mol. The rather high uncertainty level of the inferred reaction rate constant and corresponding activation energy Q_R should be emphasized. This most likely is a consequence of the observed domination of the diffusion mechanism additionally enhanced by a development of quasi-liquid layers on ice-hydrate and gas-hydrate interfaces at temperatures above 263 K. The diffusion activation energy for CH_4-hydrate formation is estimated with an uncertainty not higher than ±20%. Being comparable with previous results from the monodisperse approximation (Staykova et al. 2003), it is close to Wang's et al. (2002) estimate of 14.7 kcal/mol (61.3 kJ/mol) and practically coincides with $Q_D \approx 54.6$ kJ/mol deduced in (Genov et al. 2004) for CO_2-hydrate growth from ice powders. The similarity of activation energies for the methane and CO_2 case and the fact that the activation energy found is close to the energy of breaking hydrogen bonds in ices and hydrates suggests that the rate limiting process is the mobility of water molecules rather than the in-diffusion of the gases.

In summary, time-resolved neutron diffraction has contributed here in a crucial way to formulate a model of gas hydrate growth from ice powders which has predictive power and allows the calculation of the reaction degree as a function of temperature, pressure and grain size of a polydisperse starting material. Starting the reaction by changing the gas pressure can be done in a much faster and more precise way than changing the temperature, which permits a well-defined start of the reaction and allows to follow the first phase of the transformation with a time resolution of a few seconds. This example also demonstrates that often a detailed microstructural characterization (e.g., in terms of size distribution, particle shape and/or specific surface area) of the starting material is essential for a quantitative analysis of the diffraction results.

Anomalous preservation

Background. The last example for time-resolved neutron diffraction experiments is taken from our work on "anomalous preservation" of gas hydrates, which turned out to be related to the perfection of the ice formed during decomposition (Kuhs et al. 2004). "Anomalous preservation" (sometimes also called "self-preservation") of gas hydrates is a very intriguing phenomenon of considerable scientific and practical interest. Early observations of this effect were made independently by Davidson et al. (1986) and, more detailed, by Yakushev and Istomin (1992). These authors observed an unexpected persistence when gas hydrates were brought outside their field of stability at temperatures below the melting point of ice. More recently, Stern et al. (2001) and Takeya et al. (2001) have investigated the temperature dependency of the effect for the case of methane hydrate and found that the effect also had a lower limit. According to Stern et al. (2001) the "anomalous preservation window" extends from 240 K to the melting point of ice, while at temperatures below 240 K the decomposition is rapid and appears to be thermally activated. Within this window, the decomposition rates vary considerably by several orders of magnitude in a reproducible way (Fig. 13) with two minima at around 250 and 268 K. Takeya et al. (2002) confirmed this effect and suggested a diffusion limitation to explain the slow decomposition kinetics of gas hydrates within the anomalous preservation window. A similar, but not identical behavior was observed for CO_2 hydrate (Circone et al. 2003). Still, the deeper physical origin of "anomalous preservation" remains obscure and the controlling parameters elusive (Wilder and Smith 2002; Stern et al. 2002; Circone et al. 2004). The effect is of potential

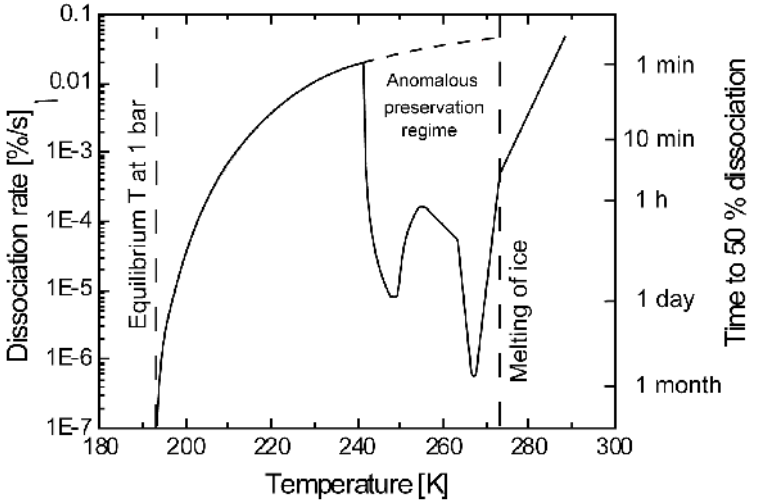

Figure 13. Temperature dependency of the decomposition rate of methane hydrate showing the region of anomalous preservation for a situation at 0.1 MPa (1 bar). [Used by permission of the Owner Societies, from Kuhs et al. (2004), Phys. Chem. Chem. Phys., Vol. 6, Fig. 1, p. 4917]

economic interest as it would allow for a low-cost compact and normal-pressure storage of gas in the form of hydrate by simple cooling to temperatures below 0°C (Gudmundsson et al. 2000) as well as it may have geological significance for some metastable surface-near gas hydrate occurrence Russian permafrost (Yakushev and Chuvilin 2000).

To be able to appreciate this connection we first turn to a discussion of the solid-solid transition of various metastable condensed forms of the water substance into ambient pressure ice. The decomposition of gas hydrates yields apparently normal ambient pressure hexagonal ice, so-called ice Ih as confirmed by Takeya et al. (2001, 2002) by laboratory X-ray diffraction. It is interesting to note that at lower temperatures various metastable solid water phases transform not into ice Ih but into so-called cubic ice, ice Ic. This form of ambient pressure ice is produced from amorphous forms of the water substance and from high-pressure ices when they are heated after a recovery at low temperature and ambient pressure (König 1943; Bertie et al. 1963) The transformation is ascribed to the on-set of mobility of Bjerrum defects promoting an ice-like crystal growth (Wooldridge et al. 1987). It was noticed early on (Arnold et al. 1968) that the diffraction patterns for ice Ic obtained from different starting materials were different. These differences were explained by Kuhs et al. (1987) in terms of various degrees of stacking faulting for ice Ic from different origins. The faults were identified as deformation stacking faults, which in diffraction experiments lead to the appearance of broad reflections at Bragg angles typical for ice Ih as well as to high- and/or low-angle shoulders on the Bragg peaks at genuine ice Ic positions. The width of the cubic reflections was used to estimate the particle size of ice Ic produced from ice II as 160 Å. Stacking faults in ice Ih and their creation by rapid temperature changes were also described by other authors (Higashi 1988) Some authors have investigated the transition of ice Ic into the normal hexagonal ice (ice Ih) by diffraction, which was found to take place over a seemingly large temperature range starting slowly at 150 K with a rapid progress of the transformation between 190 and 210 K (Kohl et al. 2000); at higher temperatures this work showed apparently pure ice Ih (Handa et al. 1986a). Differential thermal analysis of the ice Ic – ice Ih transition revealed the main transition region again at 190–205 K, with small but detectable events starting at ≈176 K (Handa et al. 1986a) and ending at ≈240 K

(Mayer and Hallbrucker 1987). A change of activation energy was observed at 185 K, and the transformation was observed to be complete at 210 K by Sugisaki et al. (1968). Already an earlier review of the situation showed a confusing picture (Hobbs 1974) in which the ice Ic – ice Ih transition was located at temperatures between 160 and 205 K, a situation which has not much improved since. Recently, additional evidence for the formation and existence of ice Ic at unusually high temperatures was established (Murray et al. 2005, Murray and Bertram 2006). The reason for such variability of the ice Ic – ice Ih transition temperatures are not clear, yet there are indications that in addition to the molecular arrangement of the parent phase mentioned above, the surface area of the ice Ic crystallites (Kumai 1968) has a significant influence. Thus it appeared worthwhile to look in some more detail at the transformation behavior of ice Ic into ice Ih in the temperature range in question with a well-defined starting material. Diffraction is the most promising tool as it permits insight into changes of the molecular arrangement not only at long ranges but also into a number of more local defect structures. In particular, time-resolved diffraction experiments allow for *in situ* studies of this transition and can give access to the transformation kinetics. Likewise, we have studied the crystallographic nature of the ice produced in decomposition of gas hydrates at temperatures below and within the anomalous preservation window by time-resolved neutron diffraction.

Experimental. The experiments were performed on the high-resolution scanning powder diffractometer D2B (wavelength 1.6 Å) as well as the high-intensity powder diffractometer D1B and D20 equipped with a linear position sensitive detector (wavelength 2.4 Å) at ILL. The first series of measurements consisted of studies of the ice Ic – ice Ih transition. The starting material used was high-pressure ice V (Lobban et al. 2000) recovered to ambient pressure at liquid nitrogen temperatures. Upon further heating at ambient pressure the recovered ice transformed into ice Ic at a temperature of 143 K within 15 h (Gotthardt 2001) Further temperature increase led to a gradual transition into ice Ih. The main structural rearrangements takes place at temperatures below 205 K in agreement with a number of previous observations (Dowell and Rinfret 1960; Kumai 1968; Handa et al. 1986a). Detailed observations were made in the temperature range between 180 and 265 K; for the experiment performed on D2B the temperature was increased at a rate of 10°/h in steps with a holding time of 30 min after reaching each target value. During both ramping and holding the temperature diffraction data were collected with a time resolution of 15 min; this is the time needed to collect data of sufficient quality to observe changes in the stacking fault arrangements by scanning with 0.05° steps in 2Θ. Particular attention was given to the peak intensity and peak shape of the cubic 111 reflection as well as the neighboring and partly overlapping hexagonal 100, 002 and 101 reflections. Intensity changes of these reflections upon heating were observed to take place first rapidly, then slowing down and coming essentially to hold. The time spent at each temperature was chosen to cover the period in which significant differences between adjacent data sets could be detected as established from exploratory runs on D20; with the good counting statistics of D20, intensity changes of 1% were detectable. The analysis of the intensity ratio of the hexagonal 100 and 002 reflection indicated the persistence of some cubic component at temperatures as high as 237 K. Following our earlier analysis (Kuhs et al. 1987) this was interpreted as cubic stacking sequences and represents the first unequivocal crystallographic evidence for the persistence of significant two-dimensional defects at temperatures above 205 K. Only at temperatures close to 240 K these imperfections finally disappear (Kuhs et al. 2004).

Independently, a number of time-resolved neutron diffraction runs were performed on the high-flux diffractometer D20 at ILL in order to study the decomposition behavior of gas hydrates. Custom-made gas pressure cells were used (Kuhs et al. 2005) which were filled with almost pure gas hydrates formed from hexagonal ice (Staykova et al. 2003). Samples were equilibrated at the desired pressure and temperature conditions. Concomitant with a pressure release to the designed end pressure, data collection was started. Again, as in the case of hydrate formation, the pressure release to the desired value (located between a few mbar and 1 bar) took

a few seconds. Consequently, this time is then the achievable time-resolution at the beginning of the process. Complete diffraction patterns were recorded with a time resolution of 10 s up to 1 min for the initial part of the reaction and slower acquisition rates of typically 5 min for the later part of the decomposition process (Fig. 14). The complete sample of typically 1 cm^3 was intercepted by the neutron beam. The analysis of the numerous diffraction data was performed in an automated fashion using the Rietveld program GSAS (Larson and von Dreele 1994) similar to the approach described for the gas hydrate formation reactions. Between 50 and 300 individual diffraction patterns were collected as a function of time for each of the decomposition runs. Beam-time restrictions limited the duration of each run to typically less than half a day.

Analysis. Quantitative information on the progress of the reaction was obtained from the phase fractions of ice and gas hydrate for each data set. The results are shown in Figure 15 for CH_4- and CO_2-hydrate. In agreement with earlier observations (Stern et al. 2001, Takeya et al. 2001) the initial decomposition was always fast, but slowed down for temperatures above approximately 240 K in the anomalous preservation regime. A phenomenological model combining an initial reaction-limited and a later diffusion-limited process can quantitatively explain the decomposition (Genov 2004). Similar successive processes also take place during the gas hydrate formation from ice as described above. More interesting in the present context is the detailed nature of the ice formed below and above the onset of anomalous preservation. A detailed inspection of the diffraction features of the ice obtained gives unequivocal evidence for the existence of stacking faults. They are clearly born out in shoulders of the main hexagonal diffraction peaks as well as in the non-ideal intensity ratio of the hexagonal 100 and 002 reflections. Insufficient crystallite statistics or textural effects can be safely excluded as an explanation of the non-ideal intensity ratios. It is noteworthy that the non-ideal character of the hexagonal ice formed is more pronounced at lower temperatures and disappears completely for all data sets in the self-preservation regime. Moreover, ice formed from CO_2- and CH_4-hydrate appears to be different in that the latter shows more pronounced features for deformation stacking faults born out in the high-angle shoulders of the hexagonal 100 reflection (Kuhs et al. 1987).

Clear evidence is found that the ice formed upon gas hydrate decomposition at temperatures below the anomalous preservation window is defective. It forms small crystallites

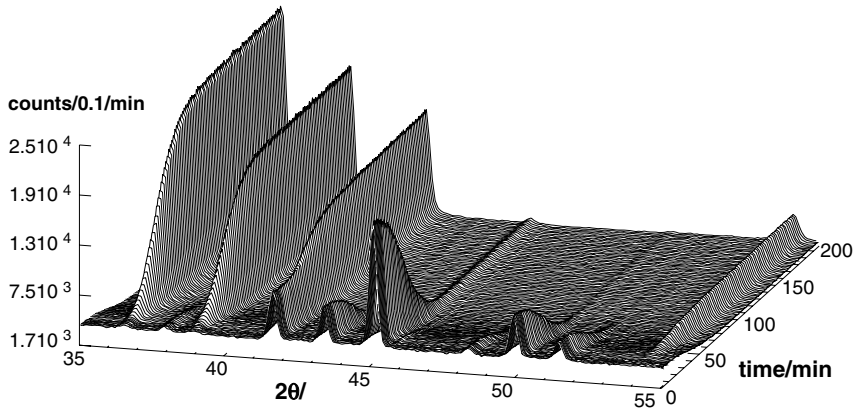

Figure 14. Stack of sequential powder diffraction patterns during decomposition of CO_2 gas hydrates. The decomposition took place at 210 K. The first 20 data acquisitions were done in 30 s each, afterwards, 199 patterns were taken in 1 min each. Thus, the whole series of sequential data acquisitions took 210 min. The counting rate per detector cell of 0.1° width in 2θ was normalized to acquisitions of 1 min.

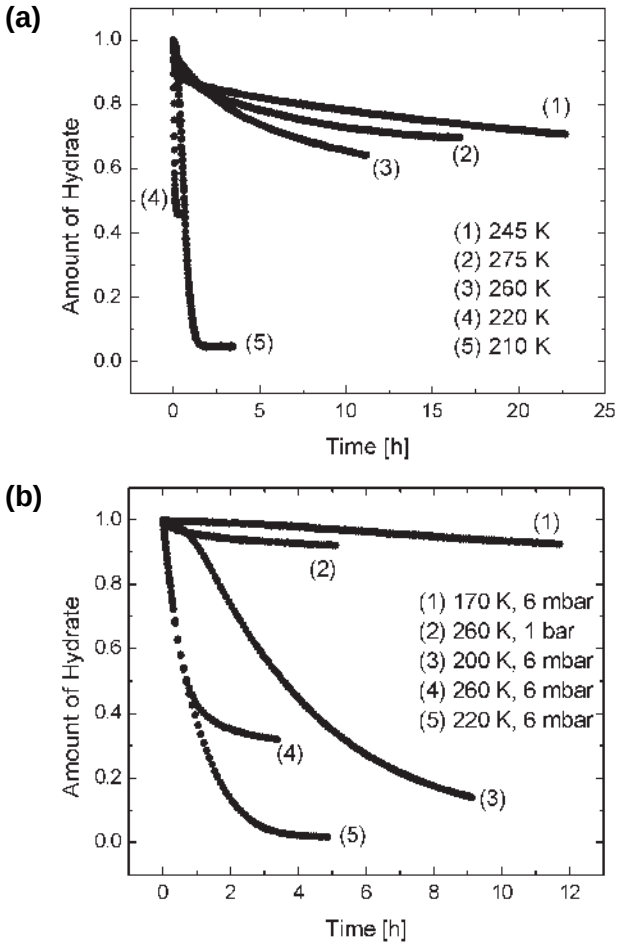

Figure 15. Time dependency of the decomposition of gas hydrate into ice shown for different temperatures. At higher temperatures the decomposition is slower due to the effect of anomalous preservation (a) CH_4 hydrate (b) CO_2 hydrate. [Used by permission of the Owner Societies, from Kuhs et al. (2004), Phys. Chem. Chem. Phys., Vol. 6, Fig. 3, p. 4919.]

of a few μm, which do not combine to larger, more homogeneous assemblies below 240 K. A complete annealing of stacking faults and appreciable grain growth of the ice crystallites sets in at temperatures of approximately 240 K. The initial amount of faults and the details of the step-wise disappearance of these stacking-faults upon temperature increase apparently depend on the parent phase as well as the speed of transformation into ice. Remarkable differences in lattice defects were established earlier on for the various high-pressure ices as parent phases (Arnold et al. 1968) In a similar way, differences in the degree of perfection were found for ice produced from decomposing CO_2 and CH_4 hydrate, with the latter showing more imperfections. As the water topology of both hydrates is identical (both form a cubic type I hydrate structure) the difference must arise from the different transformation kinetics, with CO_2 hydrate decomposing distinctly slower with a resulting less defective ice.

This example shows that a wealth of information going far beyond the perfect crystal picture is contained in diffraction data. Time-resolved studies on phase-transitions and

chemical reactions usually imply changes of the microstructure of the crystallites translating into changes in the diffraction profiles of the newly formed phases. A closer look at these details is quite often a worthwhile undertaking, but certainly also is more involved and not necessarily straightforward using existing structure analysis and refinement programs.

CONCLUSIONS AND OUTLOOK

The time-resolved work on ices and gas hydrates is by far not completed and many problems remain unsolved. So far, these studies have shown that much can be learned from truly time-resolved studies about the processes controlling structural phase transitions and chemical reactions in ices and gas hydrates. Here, we can only indicate a few further research lines of interest. Concerning the polyamorphism of ice it will be important to prove or disprove the ergodicity (time-average over one molecule in phase space identical to the space average over the ensemble considered) of the different states and time-resolved work on samples with well documented history will certainly shed further light on this issue. Most likely, diffraction, small-angle scattering and inelastic work need to be combined to really advance our understanding. Of the numerous phase transitions between the various crystalline phases of ice very few have been studied in detail. Transitions involving the restructuring of the H-bond network (usually pressure-driven) are strongly first order with considerable hysteresis. Yet, there is some evidence that topotactic relationships exist (Bennett et al. 1997), an observation which is far from being understood in detail. Time-resolved diffraction studies of textured samples may provide further insight. The usually temperature-driven proton orderings are gradual without symmetry change in some cases (ice III, ice V; Lobban et al. 2000) or abrupt and first order with symmetry changes in others (ice VII/VIII; Kuhs et al 1984). Sometimes doping is necessary to promote the proton ordering leading also to changes in symmetry as in the case of ice Ih/ice XI doped with KOH (Matsuo et al. 1986) or ices V/XIII and XII/XIV doped with HCl (Salzmann et al. 2006). It is generally accepted that Bjerrum and ionic defects in the ice lattice play an important role in the proton ordering processes (e.g., Wooldridge et al. 1987; Petrenko and Whitworth 1999) yet very little work is done to quantify the ordering processes via activation energies or molecular transport processes. Here again, time-resolved neutron diffraction studies carry considerable promise. Many open questions also prevail in the field of gas hydrates and filled ices. Hydrate formation from liquid water is certainly an issue worth looking at with diffraction methods in combination with light scattering to study the evolution of grain sizes. Two-dimensional detectors may allow in the future to follow grain sizes at larger scales also by neutron diffraction to study Ostwald ripening and related phenomena. Furthermore, it seems worthwhile to study not only the changes in Bragg intensities during a transition but also to look at phenomena like particle size broadening, induced strain or the signatures of defects like stacking faults in the peak profiles. These features call for a very good angular resolution at neutron fluxes acceptable for kinetic work. Such studies will generally need improved sources, instruments and detectors as they are under development both at reactor neutron sources such as ILL and time-of-flight facilities at LANSCE, ISIS and SNS.

Powder diffraction is a classical entrance door to neutron scattering. Experiments are easy to set up and powder samples normally readily available. Constant wavelength diffraction does not stand in direct competition to time-of-flight techniques, both techniques are complementary, and one particular advantage for time-resolved work of reactor-based diffraction is the constancy and reliability of source. The data treatment such as Rietveld refinement (Knorr and Depmeier 2006, this volume) or pair distribution function analysis (Proffen 2006, this volume) have become standardized and work efficiently with neutron powder diffraction data. Due to the penetration of neutrons, complex and unique sample environment conditions can be fairly easily adapted. Applications of time-resolved neutron diffraction techniques to unresolved problems in geology or mineralogy are numerous (see

also Redfern 2006, this volume). One has only started to discover their potential, building on earlier experiences from material science. Yet, to fully take advantages of neutron scattering one has not only to improve the performance of the instruments but also advance sample environments. Some devices are available at neutron scattering centers, others need to be built or adapted by the user to match the specific needs of kinetic work.

Finally, it should be emphasized that neutron diffraction undoubtedly gives very valuable insight into transformation kinetics, however, it provides only a time-space averaged picture of the processes. Often complementary studies using locally resolving methods like electron microscopy, tomography or other imaging techniques are needed for a complete understanding. Moreover, in a number of cases neutron wide angle diffraction may find important complements in other neutron scattering techniques, like SANS (Radlinski 2006, this volume) or quasi-elastic and inelastic scattering (Loong 2006, this volume).

ACKNOWLEDGMENTS

One author (WFK) thanks the Deutsche Forschungsgemeinschaft (DFG) and the Bundesministerium für Bildung und Forschung (BMBF) in its program GEOTECHNOLOGIEN for multiple financial support (grants 03G0553A and 03G0605B); he also thanks the ILL for hospitality during a sabbatical leave. To the work presented here a number of people have made substantial contributions which are gratefully acknowledged: Andrzej Falenty, Georgi Genov, Alice Klapproth, Doroteya Staykova from the University of Göttingen, Andrey Salamatin from Kazan State University as well as Pierre Convert and Michael M. Koza from the Institut Laue-Langevin in Grenoble. This is publication no. GEOTECH-229 in the BMBF research initiative GEOTECHNOLOGIEN.

REFERENCES

Adam G, Gibbs JH (1965) On temperature dependence of cooperative relaxation properties in glass-forming liquids. J Chem Phys 43:139-146

Arnold GP, Finch ED, Rabideau SW, Wenzel RG (1968) Neutron diffraction study of ice polymorphs III. Ice Ic. J Chem Phys 49:4365-4369

Arzt E (1982) The influence of an increasing particle coordination on the densification of spherical powders. Acta Metall 30:1883-1890

Avrami M (1939) Kinetics of phase change. I. General theory. J Chem Phys 7:1103-1112

Avrami M (1940) Kinetics of phase change. II. Transformation-time relations for random distribution of nuclei. J Chem Phys 8:212-224

Avrami M (1941) Kinetics of phase change III. Granulation, phase change, and microstructure. J Chem Phys 9:177-184

Barrer RM, Edge AVJ (1967) Gas hydrates containing argon, krypton and xenon: kinetics and energetics of formation and equilibria. Proc Royal Soc London A 300:1-24

Bellissent-Funel M-C, Teixeira J, Bosio L (1987) Structure of high-density amorphous water. II. Neutron scattering study. J Chem Phys 87:2231-2235

Bennett K, Wenk HR, Durham WB, Stern LA, Kirby SH (1997). Preferred crystallographic orientation in the ice I to II transformation and the flow of ice II. Philos Mag A 76:413-435

Berliner R, Popovici M, Herwig KW, Berliner M, Jennings HM, Thomas JJ (1998) Quasielastic neutron scattering study of the effect of water-to-cement ration on the hydration kinetics of tricalcium silicate. Cement Concrete Res 28:231-243

Bertie JE, Calvert LD, Whalley E (1963) Transformations of ice II, ice III, and ice V at atmospheric pressures. J Chem Phys 38:840-846

Besson JM, Nelmes RJ, Hamel G, Loveday JS, Weill G, Hall S (1992) Neutron powder diffraction above 10 GPa. Physica B 180-181: 907-910

Bizid A, Bosio L, Defrain A, Oumezzine M (1987) Structure of high-density amorphous water. 1. X-Ray-diffraction study. J Chem Phys 87:2225-2230

Bletry J, Taverniere P, Senillou C, Desre P, Maret M, Chieux P (1984) High temperature furnaces for small and large angle neutron scattering of disordered materials. Rev Phys Appl 19:725-730

Bosio L, Johari GP, Teixeira J (1986) X-ray study of high-density amorphous water. Phys Rev Lett 56:460-463

Bray HJ, Redfern SAT (1999) Kinetics of dehydration of Ca-montmorillonite. Phys Chem Minerals 26:591-600

Brown ABD, Clarke SM (2000) Orientational order in concentrated dispersions of plate-like kaolinite particles under shear. J Rheology 44(2):221-233

Brown ABD, Clarke SM, Rennie AR (1998) Shear induced alignment of kaolinite: studies using a diffraction technique. Prog Colloid Polymer Sci 110:80-82

Chazallon B, Kuhs WF (2002) *In situ* structural properties of N_2-, O_2-, and air-clathrates by neutron diffraction. J Chem Phys 117:308-320

Circone S, Stern LA, Kirby SH (2004) The role of water in gas hydrate dissociation. J Phys Chem B 108: 5747-5755

Circone S, Stern LA, Kirby SH, Durham WB, Chakoumakos BC, Rawn CJ, Rondinone AJ, Ishii Y (2003) CO_2 hydrate: synthesis, composition, structure, dissociation behavior and comparison to structure I CH_4 hydrate. J Phys Chem B107:5529-5539

Cole DR, Herwig KW, Mamontov E, Larese J (2006) Neutron scattering and diffraction studies of fluids and fluid-solid interactions. Rev Mineral Geochem 63:313-362

Convert P, Berneron M, Gandelli R, Hansen TC, Oed A, Rambaud A, Ratel J, Torregrossa J (1997) A large high counting rate one-dimensional position sensitive detector: the D20 banana. Physica B234:1082-1083

Convert P, Hansen T, Oed A, Torregrossa J (1998) D20 high-Flux two-axis neutron diffractometer. Physica B241-243:195-197

Convert P, Hansen T, Torregrossa J (2000) The high intensity two axis neutron diffractometer D20 first results. Mater Sci Forum 321-324:314-319

Convert P, Hock R, Vogt T (1990) High-speed time-resolved crystallography with neutrons - a feasibility study. Nucl Instrum Methods Phys Res A 292:731-733

Crank J (1975) The Mathematics of Diffusion. Clarendon Press

Davidson DW, Garg SK, Gough SR, Handa YP, Ratcliffe CI, Ripmeester JA, Tse JS, Lawson WF (1986) Laboratory analysis of a naturally occurring gas hydrate from sediments of the Gulf of Mexico. Geochim Cosmochim Acta 50:619-623

Debye P, Bueche AM (1949) Scattering by an Inhomogeneous Solid. J Appl Phys 20:518-525

Doremus RH (1985) Rates of Phase Transitions. Academic

Dowell LG, Rinfret AP (1960) Low-temperature forms of ice as studied by X-ray diffraction. Nature 188: 1144-1148

Erofeyev BV (1946) A generalized equation of chemical kinetics and its application in reactions involving solids. Dokl Akad Nauk SSSR 52:511-514

Fehr KT, Huber M, Zuern SG, Peters E. (2003) Determination of the reaction kinetics and reaction mechanisms of Al-tobermorite under hydrothermal conditions by in-situ neutron diffraction. *In:* Hydrothermal Reactions and Techniques. Feng SH, Chen JS, Shi, Z (eds) World Scientific, p 19-26

Fei Y, Wang Y (2001) High-pressure and high-temperature powder diffraction. Rev Mineral Geochem 41: 521-558

Floriano MA, Whalley E, Svensson EC, Sears VF (1986) Structure of high-density amorphous ice by neutron diffraction. Phys Rev Lett 57:3062-3064

Froment GF, Bischoff KB (1990) Chemical Reactor Analysis and Design. Wiley & Sons

Fujii K, Kondo W (1974) Kinetics of hydration of tricalcium silicate. J Am Ceram Soc 57:492-497

Geiger A, Stanley HE (1982) Low-density patches in the hydrogen-bonded network of liquid water: Evidence from molecular dynamics computer simulations. Phys Rev Lett 49:1749-1752

Genov G (2004) Physical processes of the CO_2 hydrate formation and decomposition at conditions relevant to Mars. Doctoral Thesis, Georg-August-Universität, Göttingen

Genov G, Kuhs WF, Staykova DK, Goreshnik E, Salamatin AN (2004) Experimental studies on the formation of porous gas hydrates. Am Mineral 89:1229-1239

Gotthardt F (2001) Phasenverhalten und Phasenumwandlungen im Eis bei Gegenwart der Gase Helium, Neon und Argon. Doctoral Thesis, Georg-August-Universität, Göttingen

Grimsditch M (1986) Annealing and relaxation in the high-pressure phase of amorphous SiO_2. Phys Rev B 34:4372-4373

Gudmundsson A, Andersson V, Levik OI, Mork M (2000) Hydrate technology for capturing stranded gas. Ann N Y Acad Sci 912:403-410

Halpern Y, Thieu V, Henning RW, Wang X, Schultz AJ (2001) Time-resolved *in situ* neutron diffraction studies of gas hydrate: Transformation of structure II (sII) to structure I (sI) J Am Chem Soc 123:12826-12831

Hancock JD, Sharp JH (1972) Method of comparing solid- state kinetic data and its application to the decomposition of kaolinite, brucite, and $BaCO_3$. J Am Ceram Soc 55:74-77

Handa YP, Klug DD (1988) Heat capacity and glass transition behavior of amorphous ice. J Phys Chem 92: 3323-3325

Handa YP, Klug DD, Whalley E (1986a) Difference in energy between cubic and hexagonal ice. J Chem Phys 84:7009-7010
Handa YP, Mishima O, Whalley E (1986b) High-density amorphous ice. III. Thermal properties. J Chem Phys 84:2766-2770
Hannon AC (2005) Results on disordered materials from the General Materials diffractometer, GEM, at ISIS. Nucl Instrum Methods Phys Res A 551:88-107
Hansen TC (2004) Future trends in high intensity neutron powder diffraction. Mater Sci Forum 443-444: 181-186
Henning RW, Schultz AJ, Thien V, Halpern Y (2000) Neutron diffraction studies of CO_2 clathrate hydrate: formation from deuterated ice. J Phys Chem 104:5066-5071
Hewat AW (2006) High flux diffractometers on reactor neutron sources. Physica B 385-396, doi:10.1016/j.physb.2006.05.316
Higashi A (1988) Lattice Defects in Ice Crystals. X-ray Topographic Observations. Hokkaido Univ. Press
Hobbs PV (1974) Ice Physics, Clarendon Press
Hodges JP (2004) POWGEN3: A high resolution third generation TOF powder diffractometer under construction at the SNS. J Minerals Metals Materials Society 56:206
Holland-Moritz D, Schenk T, Herlach DM, Convert P, Hansen T (2005) Electromagnetic levitation apparatus for diffraction investigations on the short-range order of undercooled metallic melts. Meas Sci Technol 16:372-380
Hondoh T, Uchida T (1992) Formation process of clathrate air-hydrate crystals in polar ice sheets. Teion Kagaku [Low Temperature Science] A51:197-212
Howard JAK, Johnson O, Schultz AJ, Stringer AM (1987) Determination of the Neutron Absorption Cross Section for Hydrogen as a Function of Wavelength with a Pulsed Neutron Source. J Appl Cryst 20:120-122
Hwang MJ, Wright DA, Kapur A, Holder GD (1990) An experimental study of crystallization and crystal growth of methane hydrates from melting ice. J Inclus Phenom 8:103-116
Johari GP (1976) The dielectric properties of H_2O and D_2O ice Ih at MHz frequencies. J Chem Phys 64:3998-4005
Johari GP (1995) Phase transition and entropy of amorphous ices. J Chem Phys 102:6224
Johari GP, Hallbrucker A, Mayer E (1987) The glass-liquid transition of hyperquenched water. Nature 330: 552-553
Johari GP, Hallbrucker A, Mayer E (1991) Isotope and impurity effects on the glass-transition and crystallization of pressure-amorphized hexagonal and cubic ice. J Chem Phys 95:6849-6855
Johari GP, Jones SJ (1976) Dielectric properties of polycrystalline D_2O ice Ih (hexagonal). Proc Roy Soc London A349:467-495
Johari GP, Jones SJ (1978) The orientation polarization in hexagonal ice parallel and perpendicular to the c-axis. J Glaciology 21:259-276
Kargel JS (2004) Mars; a Warmer, Wetter Planet. Springer
Karpov VG, Grimsditch M (1993) Pressure-induced transformations in glasses. Phys Rev B48:6941-6948
Kashchiev D (2000) Nucleation. Basic Theory with Applications. Butterworth-Heineman
Khvostantsev LG, Slesarev VN, Brazhkin VV (2004) Toroid type high-pressure device: history and prospects. High Press Res 24: 371-385
Kilcoyne SH, Manuel P (2002) A kinetic neutron diffraction study of the crystallisation of α-Er_7Fe_3. Appl Phys A-Mater 74:S1166-S1168
Klapproth A (2002) Strukturuntersuchungen an Methan- und Kohlenstoffdioxid-Clathrat-Hydraten. Doctoral Thesis, Georg-August-Universität, Göttingen
Klapproth A, Goreshnik E, Staykova DK, Klein H, Kuhs WF (2003) Structural studies of gas hydrates. Can J Phys 81:503-518
Knorr K, Depmeier W (2006) Application of neutron powder-diffraction to mineral structures. Rev Mineral Geochem 63:99-111
Kohl I, Mayer E, Hallbrucker A (2000) The glassy water - cubic ice system: a comparative study by X-ray diffraction and differential scanning calorimetry. Phys Chem Chem Phys 2:1579-1586
Kolmogorov AN (1937) On the statistical theory of metal crystallization. Izv Akad Nauk SSR Ser Mat 3: 355-359
König H (1943) Eine kubische Eismodifikation. Z Kristallogr 105:279-286
Koza M, Schober H, Toelle A, Fujara F, Hansen T (1999) Formation of ice XII at different conditions. Nature 397:660-661
Koza MM, Geil B, Winkel K, Köhler C, Czeschka F, Scheuermann M, Schober H, Hansen T (2005) Nature of amorphous polymorphism of water. Phys Rev Lett 94:125506(4)
Koza MM, Hansen T, May R, Schober H (2006) Link between the diversity, heterogeneity and kinetic properties of amorphous ice structures. J Non-Cryst Solids, doi:10.1016/j.jnoncrysol.2006.02.162

Koza MM, Schober H, Fischer HE, Hansen T, Fujara F (2003) Kinetics of the high- to low-density amorphous water transition. J Phys Condens Matt 15:321-332
Koza MM, Schober H, Hansen T, Toelle A, Fujara F (2000) Ice XII in its second regime of metastability. Phys Rev Lett 84:4112-4115
Kuhs WF (2003) Atomic displacement parameters. *In:* International Tables for Crystallography, D: Physical Properties of Crystals. Authier A (ed), IUCr, Kluwer, p 228-242
Kuhs WF (2004) The high pressure crystallography of gas hydrates. *In:* High-Pressure Crystallography. Katrusiak A, McMillan P (eds) Kluwer, p 475-494
Kuhs WF, Bliss DV, Finney JL (1987) High-resolution neutron powder diffraction study of ice Ic. J Phys Coll C1 Paris 48:631-636
Kuhs WF, Finney JL, Vettier C, Bliss DV (1984) Structure and hydrogen ordering in ices VI, VII, and VIII by neutron powder diffraction. J Chem Phys 81:3612-3623
Kuhs WF, Genov G, Staykova DK, Hansen TC (2004) Ice perfection and onset of anomalous preservation of gas hydrates. Phys Chem Chem Phys 6:4917-4920
Kuhs WF, Hensel E, Bartel H (2005) Gas pressure cells for elastic and inelastic neutron scattering. J Phys Condens Matter 17: 3009-3015
Kuhs WF, Klapproth A, Gotthardt F, Techmer K, Heinrichs T (2000) The formation of meso- and macroporous gas hydrates. Geophys Res Lett 27:2929-2932
Kuhs WF, Staykova DK, Salamatin AN (2006) Formation of methane hydrate from polydisperse ice powders: Long-term experiments. J Phys Chem B 110:13283-13295
Kumai M (1968) Hexagonal and cubic ice at low temperature. J Glaciology 7:95-108
Larson AC, von Dreele RB (1990) Los Alamos National Laboratory. Report No. LAUR 86-748
Lasaga AC (1998) Kinetic Theory in the Earth Sciences. Princeton University Press
Latroche M, Chabre Y, Decamps B, Percheron-Guegan A, Noreus D (2002) *In situ* neutron diffraction study of the kinetics of metallic hydride electrodes. J Alloy Compd 334:267-276
Levenspiel O (1999) Chemical Reaction Engineering. Wiley & Sons
Lobban C, Finney JL, Kuhs WF (1998) The structure of a new phase of ice. Nature 391:268-270
Lobban C, Finney JL, Kuhs WF (2000) The structure and ordering of ices III and V. J Phys Chem 112:7169-7180
Loerting T, Salzmann C, Kohl I, Mayer E, Hallbrucker A (2001) A second distinct structural "state" of high-density amorphous ice at 77 K and 1 bar. Phys Chem Chem Phys 3:5355-5357
Loerting T, Schustereder W, Winkel K, Salzmann CG, Kohl I, Mayer E (2006) Amorphous ice: Stepwise formation of very-high-density amorphous ice from low-density amorphous ice at 125 K. Phys Rev Lett 96:025702-025704
Lokshin KA, Zhao Y (2005) Advanced setup for high-pressure and low-temperature neutron diffraction at hydrostatic conditions. Rev Sci Instrum 76:063909
Loong C-K (2006) Inelastic scattering and applications. Rev Mineral Geochem 63:233-254
Lorenz G, Neder RB, Marxreiter J, Frey F, Schneider J (1993) Mirror furnace for neutron diffraction up to 2300 K. J Appl Crystallogr 26:632-635
Lundgaard L, Mollerup J (1992) Calculation of phase diagrams of gas-hydrates, Fluid Phase Equil 76:141-149.
Matsuo T (2003) Quantum aspects of low-temperature properties of crystals: A calorimetric study in interaction with spectroscopy and diffraction. Pure Appl Chem 75:913-926
Matsuo T, Tajima Y, Suga H (1986) Calorimetric study of a phase transition in D_2O ice Ih doped with KOD: ice XI. J Phys Chem Solids 47:165-173
Max MD (ed) (2003) Natural Gas Hydrate in Oceanic and Permafrost Environments. Kluwer Academic Publishers
Max MD, Johnson AH, Dillon WP (eds) (2006) Economic Geology of Natural Gas Hydrate. Springer, Dordrecht
Mayer E, Hallbrucker A (1987) Cubic ice from liquid water. Nature 325:601-602
Mishima O (1994) Reversible first-order transition between two H_2O amorphs at 0.2 GPa and 135 K. J Chem Phys 100:5910-5912
Mishima O (1996) Relationship between melting and amorphization of ice. Nature 384:546-549
Mishima O, Calvert LD, Whalley E (1984) An apparently first-order transition between two amorphous phases of ice induced by pressure. Nature 310:393-395
Mishima O, Calvert LD, Whalley E (1985) Phase behaviour of metastable water. Nature 314:76-78
Mishima O, Stanley HE (1998) The relationship between liquid, supercooled and glassy water. Nature 396: 329-335
Mishima O, Takemura K, Aoki K (1991) Visual observations of the amorphous-amorphous transition in H_2O under pressure. Science 254:406-408
Mizuno Y, Hanafusa N (1987) Studies of surface properties of ice using nuclear magnetic resonance. J Phys Coll C1 Paris 48: 511-517

Murray BJ, Bertram AK (2006) Formation and stability of cubic ice in water droplets. Phys Chem Chem Phys 8:186-192
Murray BJ, Knopf DA, Bertram AK (2005) The formation of cubic ice under conditions relevant to Earth's atmosphere. Nature 434:202-205
Oed A (1988) Position-sensitive detector with microstrip anode for electron multiplication with gases. Nucl Instrum Methods Phys Res A 263:351-359
Pannetier J (1985) Time-Resolved Neutron Powder Diffraction. Chem Sci 26A:131-139
Parise JB (2006a) Introduction to neutron properties and applications. Rev Mineral Geochem 63:1-25
Parise JB (2006b) High pressure studies. Rev Mineral Geochem 63:205-231
Peterson RC, Yang H (2001) High-temperature devices and experimental cells for X-ray and neutron diffraction experiments. Rev Mineral Geochem 41:425-444
Petrenko VF and Whitworth RW (1999) Physics of Ice. Oxford University Press, Oxford.
Poole PH, Grande T, Austen Angell C, Sciortino F, Eugene Stanley H (1994) Effect of hydrogen bonds on the thermodynamic behavior of liquid water. Phys Rev Lett 73:1632-1635
Poole PH, Sciortino F, Essmann U, Stanley HE (1992) Phase behaviour of metastable water. Nature 360:324-328
Pradell T, Crespo D, Clavaguera N, Clavaguera-Mora, MT (1998) Diffusion controlled grain growth in primary crystallization. Avrami exponents revisited. J Phys Cond Matter 10:3833-3844
Primak W (1975) The Compacted States of Vitreous Silica. Gordon and Breach
Proffen T (2006) Analysis of disordered materials using total scattering and the atomic pair distribution function. Rev Mineral Geochem 63:255-274
Pruzan P, Chervin JC, Wolanin E, Canny B, Gauthier M, Hanfland M (2003) Phase diagram of ice in the VII-VIII-X domain. Vibrational and structural data for strongly compressed ice VIII. J Raman Spectroscopy 34:591-610
Radaelli PG, Hannon AC, Chapon LC (2003) GEM: A Shining Light in the ISIS Crown. Notiz Neut Luce Sinc 8:19-26
Radlinski AP (2006) Small-angle neutron scattering and the microstructure of rocks. Rev Mineral Geochem 63:363-397
Redfern SAT (2006) Neutron powder diffraction studies of order-disorder phase transitions and kinetics. Rev Mineral Geochem 63:145-170
Riekel C, Schöllhorn R (1976) A neutron diffraction study on the intercalation of ammonia into tantalum disulfide. Mater Res Bull 11:369-376
Riley DP, Kisi EH, Hansen TC, Hewat AW (2002) Self-propagating high-temperature synthesis of Ti_3SiC_2: I, ultra-high-speed neutron diffraction study of the reaction mechanism. J Am Ceram Soc 85:2417-2424
Riley DP, Oliver CP, Kisi EH (2006) In-situ neutron diffraction of titanium silicide, Ti_5Si_3, during self-propagating high-temperature synthesis (SHS). Intermetallics 14:33-38
Röttger K, Endriss A, Ihringer J, Doyle S, Kuhs WF (1994) Lattice constants and thermal expansion of H_2O and D_2O ice Ih between 10 and 265 K. Acta Crystallogr B 50:644-648
Salamatin AN, Hondoh T, Uchida T, Lipenkov VY (1998) Post-nucleation conversion of an air bubble to clathrate air-hydrate crystal in ice. J Cryst Growth 193:197-218
Salamatin AN, Kuhs WF (2002) Formation of porous gas hydrates. Proc Fourth Int Conf Gas Hydrates, Yokohama 766-770
Salzmann CG, Radaelli PG, Hallbrucker A, Mayer E, Finney, JL (2006) The preparation and structures of hydrogen ordered phases of ice. Science 311:1758-1761
Sastry S, Sciortino F, Stanley HE (1993) Limits of stability of the liquid phase in a lattice model with water-like properties. J Chem Phys 98:9863-9872
Schmitt B, de Bergh C, Festou M (eds) (1998) Solar System Ices. Astrophysics and Space Science Library 227. Kluwer Academic Publishers
Schmitt D, Ouladdiaf ,B (1998) Absorption correction for annular cylindrical samples in powder neutron diffraction. J Appl Crystallogr 31:620-624
Schober H, Koza M, Toelle A, Fujara F, Angell CA, Boehmer R (1998) Amorphous polymorphism in ice investigated by inelastic neutron scattering. Physica B241-243:897-902
Sciortino F, Tartaglia P (2001) Aging in simple liquids: A numerical study. J Phys Cond Matter 13:9127-9140
Sears VF (1992) Neutron scattering lengths and cross sections. Neutron News 3:29-37
Sloan ED Jr (1998) Clathrate Hydrates of Natural Gases. Marcel Dekker, Inc.
Sloan ED Jr, Fleyfel F (1991) A molecular mechanism for gas hydrate nucleation from ice. Inst Chem Eng J 37:1281-1292
Speedy RJ (1982) Limiting forms of the thermodynamic divergencies at the conjectured stability limit in superheated and supercooled water. J Phys Chem 86:3002-3005
Speedy RJ (1982) Stability-limit conjecture. An interpretation of the properties of water. J Phys Chem 86: 982-991

Stanley HE, Teixeira J (1980) Interpretation of the unusual behavior of H_2O and D_2O at low temperatures: Tests of a percolation model. J Chem Phys 73:3404-3422

Staykova DK, Kuhs WF, Salamatin AN, Hansen T (2003) Formation of porous gas hydrates from ice powders: Diffraction experiments and multi-stage model. J Phys Chem B107:10299-10311

Stern LA, Circone S, Kirby SH, Durham WB (2001) Anomalous preservation of pure methane hydrate at 1 atm. J Phys Chem B105:1756-1762

Stern LA, Circone S, Kirby SH, Durham WB (2002) Reply to "Comments on 'Anomalous preservation of pur methane hydrate at 1 atm'." J Phys Chem B106:228-330

Stern LA, Hogenboom DL, Durham WB, Kirby SH, Chou IM (1998) Optical-cell evidence for superheated ice under gas-hydrate-forming conditions. J Phys Chem B102:2627-2632

Sugisaki M, Suga H, Seki S (1968) Calorimetric study of the glassy state. IV: Heat capacities of glassy water and cubic ice. Bull Chem Soc Japan 41:2591-2599

Takeya S, Ebinuma T, Uchida T, Nagao J, Narita H (2002) Self-preservation effect and dissociation rates of CH_4 hydrate. J Cryst Growth 237-239:379-382

Takeya S, Hondoh T, Uchida T (2000) In-situ observations of CO_2 hydrate by X-ray diffraction. Ann N Y Acad Sci 912:973-982

Takeya S, Shimada W, Kamata Y, Ebinuma T, Uchida T, Nagao J, Narita H (2001) In-situ X-ray diffraction measurements of self-preservation effect of CH_4 hydrate. J Phys Chem A105:9756-9759

Tanaka H (2000) Thermodynamic anomaly and polyamorphism of water. Europhys Lett 50:340-346

Tsiok OB, Brazhkin VV, Lyapin AG, Khvostantsev LG (1998) Logarithmic kinetics of the amorphous-amorphous transformations in SiO_2 and GeO_2 glasses under high pressure. Phys Rev Lett 80:999-1002

Uchida T, Hondoh T, Mae S, Duval P, Lipenkov VY (1992) In-situ observations of growth process of clathrate air-hydrate under hydrostatic pressure. *In:* Physics and Chemistry of Ice. Maeno N, Hondoh T (eds) Hokkaido University Press, p 121-125

Uchida T, Hondoh T, Mae S, Duval P, Lipenkov VY (1994) Effects of temperature and pressure on transformation rate from air-bubbles to air-hydrate crystals in ice sheets. Ann Glaciology 20:143-147

Velikov V, Borick S, Angell CA (2001) The glass transition of water, based on hyperquenching experiments. Science 294:2335-2338

von Stackelberg M, Müller HR (1954) Feste Gashydrate II: Struktur und Raumchemie. Z Elektrochemie 58: 25-39

Walk-Lauffer B (2003) Untersuchung des Einflusses von Sulfaten auf das System CaO-SiO_2-Al_2O_3-K_2O-H_2O mittels Wärmeflusskalorimetrie und in-situ Neutronenbeugung unter hydrothermalen Bedingungen. Dissertation, Universität Siegen, Logos Verlag

Walton RI, Francis RJ, Halasyamani PS, O'Hare D, Smith RI, Done R, Humphreys RJ (1999) Novel apparatus for the *in situ* study of hydrothermal crystallizations using time-resolved neutron diffraction. Rev Sci Instrum 70:3391-3396

Walton RI, Millange F, Smith RI, Hansen TC, O'Hare D (2001) Real time observation of the hydrothermal crystallization of barium titanate using *in situ* neutron powder diffraction. J Am Chem Soc 123(50): 12547-12555

Wang X, Schultz AJ, Halpern Y (2002) Kinetics of methane hydrate formation from polycrystalline deuterated ice. J Phys Chem A 106:7304-7309

Warzinski RP, Lynn, RJ Holder GD (2000) The impact of CO_2 clathrate hydrate on deep ocean sequestration of CO_2. Ann N Y Acad Sci 912:226-234

Wilder JW, Smith DH (2002) Comments on "Anomalous preservation of pure methane hydrate at 1 atm." J Phys Chem B106:226-227

Wilding MC, Benmore CJ (2006) Structure of glasses and melts. Rev Mineral Geochem 63:275-311

Williams WG, Ibberson RM, Day P, Enderby JE (1998) GEM - General Materials Diffractometer at ISIS. Physica B241-243:234-236

Wooldridge PJ, Richardson HH, Devlin JP (1987) Mobile Bjerrum defects: A criterion for ice-like crystal growth. J Chem Phys 87:4126-4131

Yakushev VS, Chuvilin EM (2000) Natural gas and hydrate accumulation within permafrost in Russia. Cold Regions Sci Technol 31:189-197

Yakushev VS, Istomin VA (1992) Gas-hydrate self-preservation effect. *In:* Physics and Chemistry of Ice. Maeno N, Hondoh T (eds) Hokkaido University Press, p 136-140

Yershov ED (2004) General Geocryology. Cambride Univ Press